Master Thesis

Calibration of the 10inch PMT

for IceCube Experiment

03UM1106

Kazuhiro Fujimoto

A thesis submitted in partial fulfillment
of the requirements of the degree of Master of
Science

at

Graduate School of Science and Technology

Chiba University

Contents

List of Figures

List of Tables

Abstract

The IceCube Cherenkov detector is using photo multiplier tubes (PMTs) at Antarctic Pole for detecting extraterrestrial high energy neutrino. Inside the Earth, neutrinos are converted into charged leptons via the weak nuclear interaction, emitting Cherenkov light which is detectable by PMTs in ice at Antarctic Pole.

It is very important to calibrate the PMTs before detector deployment and data-taking. For that purpose, I have measured basic performances of the PMTs. In concrete form, I have measured charge response, waveform data and noise rate at temperature of -32 degree expected in the actual operation environment.

The charge response measurement includes voltage dependence of gain, charge resolution and, Peak to valley ratio. Waveform of PMT pulses has been modeled by the analytical formula with Gaussian. Noise rate has been also measured by removal of after pulse and ringing component.

All PMTs we have examined are found to be satisfied with the following the IceCube criteria. 1×10^7 at less than 2000V for gain, 0.20 to 0.35 at gain of 5×10^7 for $\Delta Q / Q$, P / V ranged between 2.3 and 6.8 at 5×10^7. Pulse width of waveform measurement is 1.85 to 2.33 [ns] at 5×10^7.

Chapter 1

Introduction to IceCube

1.1   Introduction of EHE Neutrino Astrophysics

Up to now, people have looked up the sky to study the structure and history of the universe and the heavenly bodies. At beginning of 17 century, Galileo Galilei who was born in the Netherlands invented a astronomical telescope, exploring the Universe by using visible light. Photon radiation has been continuously seen by a series of observations in the electric wave region, from the X rays up to the gamma rays. It should be remarked, however, that we are not able to see extremely high energy charged particle because they interact with cosmic microwave background (CMB). Neutrinos can directly arrive on the earth from the source, however, because neutrinos have no charge and they are subject only to week interactions.

The extremely high energy(EHE) neutrinos with energies up to 10^{20} eV may be produced by Greisen-Zatsepin-Kuzmin(GZK) mechanism. The GZK neutrinos are generated via decays of charged pions produced by photo-pion production of EHE cosmic rays(EHECRs) colliding cosmic microwave background(CMB) photons. This GZK mechanism is represented by the following reactions.

$$p\gamma_{CMB} \quad \longrightarrow \quad \pi^{\pm} + anything \tag{1.1}$$

$$\longrightarrow \quad \nu^{\pm} + \nu_{\mu}(\bar{\nu}_{\mu}) \tag{1.2}$$

$$\longrightarrow \quad e^{\pm} + \nu_e(\bar{\nu}_e + \bar{\nu}_{\mu}(\nu_{\mu})) \tag{1.3}$$

In this production mechanism, ν_{τ} is not originally generated. Therefore primary neutrinos should consist of $\nu_e : \nu_{\nu} : \nu_{\tau} = 1 : 2 : 0$. But considering neutrino oscillations, this ratio

1

becomes 1 : 1 : 1 after their cosmologically long flight before their arrival at earth. This phenomenon is especially interesting for neutrino telescopes because the ν_τ would not absorbed in the Earth due to the charged regeneration effect.

1.2 Neutrino Sources

Although no high energy neutrino sources have been detected at the present time, the list of candidates can be very long. It ranges from the guaranteed galactic emissions by cosmic ray interactions in the Galactic Plane, to the prime suspects like AGNs, GRBs and the GZK, and to exotic sources like topological defects. While the cleanest signature for an observation of extraterrestrial neutrinos would be a point-like hot spot on a neutrino sky map, the present resolution of neutrino telescopes requires very bright neutrino sources for an indisputable detection. A complement to a point source signal is a diffuse extraterrestrial neutrino signal, whose detection hinges on its separation from the atmospheric neutrinos opens a large window for discovery, even integrated source fluxes are orders of magnitude below the background. Since the majority of proposed extraterrestrial neutrino sources have energy spectrum significantly harder than $E^{-3.7}$, the use of very high energy neutrinos opens a large window for discovery, even if the integrated source fluxes are orders of magnitude below the background.

1.3 Detection Method

Since the cross sections of the neutrino interaction in high energy range are enhanced, they are likely to interact with the nuclei (N) of medium in the earth and produce secondary neutrinos or charged leptons via neutral current interaction (NC) or charged current interaction (CC),

$$\nu_l(\bar{\nu}_l) + N \quad \longrightarrow \quad \nu_l(\bar{\nu}_l) + X(NC); \tag{1.4}$$

$$\nu_l(\bar{\nu}_l) + N \quad \longrightarrow \quad l^{\mp} + X(CC); \tag{1.5}$$

where N is a nucleon of the medium, l is charged lepton (e,μ,τ), X is produced hadrons.

Hadrons produced via NC or CC induce a hadronic cascade, and an electron produced via CC initiates an electromagnetic cascade. Therefore EHE particles arriving at an underground

detector (*IceCube*) are not primary neutrinos, but secondary produced $\nu's$, $\mu's$ and $\tau's$.

The Cherenkov light is emitted, when a charged particle propagates in transparent medium with the speed faster than that of light in the medium. The number of radiated photons is proportional to path length, and the emission angle depends on the refractive index of the medium. By seeing emitted Cherenkov light and its angle, we can detect the charged particle and reconstruct the event track originated in neutrinos.

1.4 The IceCube Detector

IceCube is a one-cubic-kilometer international high-energy neutrino observatory being built and installed in the clear deep ice at the South Pole. IceCube will open unexplored bands for astronomy, particle physics, including the PeV (10^{15} eV) energy region, where the Universe is opaque to high energy gamma rays originating from beyond the edge of our own galaxy, and where cosmic rays do not carry directional information because of their deflection by magnetic fields. IceCube will provide a totally novel viewpoint on the multi-messenger astronomy of gamma ray bursts, which have been identified as a possible source of the highest energy particles in nature.

1.4.1 Ice as The Detector Medium

The glacial ice at the South Pole is the cleanest and the most transparent naturally occurring substance known to human being. The concentration of impurities (including radioactive particles) ranges from ~200 to 500 ng/g. Its purity and the low temperature (~-20 degree) between depths of 1500 ~ 2000m) provide the most ideal environment on the Earth for operation of photomultiplier tubes.
The ice also offers a stable base of operations for the detector installation, operation, and maintenance. Even if routing signals through 2 km of cables frozen in ice might sound troublesome by accelerator physics standards, it is simpler than the case where tens of kilometers of submarine cable are needed to bring signals from water-based detectors to the store.

1.4.2   Instrumentation
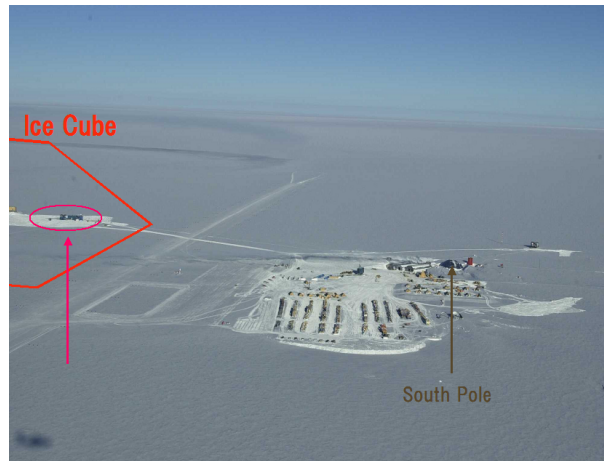
Figure 1.1: Location of IceCube

IceCube Detector for neutrino telescope is an array of 4800 Photo Multiplier Tubes (PMTs) each enclosed in a transparent pressure sphere to comprise an Optical Module(OM) similar to those in AMANDA, a small pioneering detector already in operation at South Pole. In the case of AMANDA, received analog signal from PMT directly sent to host PC, but in the case of IceCube, signal can be clearly because the Analog Transient Waveform Digitize (ATWD) of Digital Optical Module (DOM) convert analog of PMT's signal into digital. In IceCube, 80 Strings are regularly spaced by 125m over an area of approximately one square kilometer, with OMs at depths of 1400 to 2400 m below the surface. A string contains 60 DOMs spaced by 17m. Each string consists of OMs connected electrically and mechanically to a long cable. The signal cables from all the string are brought to a central location.

Each DOM contains a PMT that detects individual photons of Cherenkov light generated in the optically clear ice by mesons and electrons moving with velocities near the speed of light. Signal event consist mainly of up-going muons produced in neutrino interactions in the bedrock or the ice. The detector can receive Cherenkov photons from electromagnetic and hadronic showers (cascades) generated by interactions of ν_e and ν_τ or secondary produced μ and τ inside the detector volume provided they are sufficiently energetic. Background events are mainly down-going muons from cosmic ray interactions in the atmosphere above the detector. This background is monitored for calibration purposes by the IceTop air shower array

4
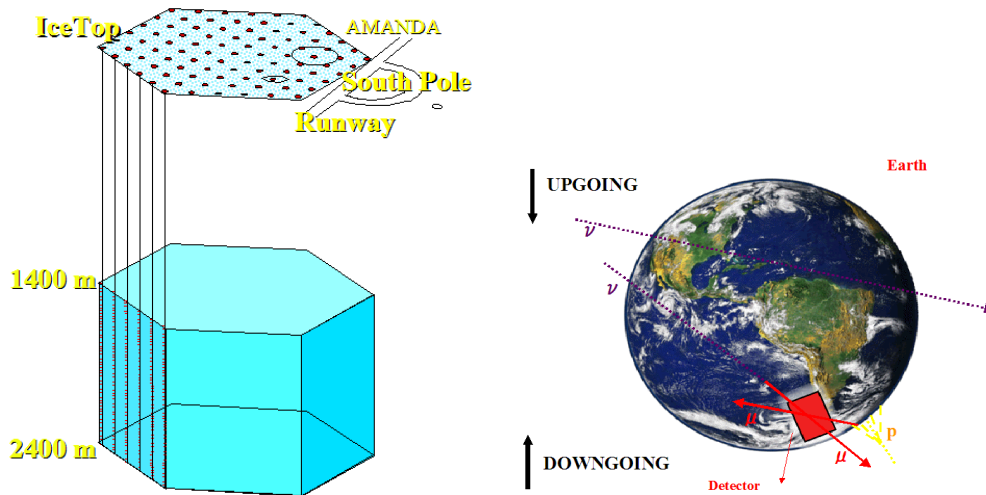
Figure 1.2: Left:Configuration of the IceCube observatory. Right:IceCube Event topology.

covering the Cherenkov light detector.

The Digital Optical Module (DOM) is a self-contained data acquisition platform. DOM is to capture and to digitize real-time PMT waveform, when requested to store data internally, and to transmit them to the surface data acquisition (DAQ) system. DAQ system has its own processor, memory, flash file system, and Real-Time Operating System (RTOS).

This DOM can be scheduling background communication tasks while acquiring data from a local waveform digitizer. All calibration functions needed to interpret data for physical content may be invoked under software control. Some operate as scheduled tasks without interfering with data acquisition, and others require dedicated control of state.

A Field Programmable Gate Array (FPGA) is used to implement most low-level logical functions of the DOM, facilitating fully programmable and flexible implementation of performance features. The FPGA is programmed automatically from a configuration file that the CPU retrieves from flash memory in the DOM after power-up and self-boot has occurred. The FPGA design and CPU programs can be replaced at will subsequent to deployment to enhance functionally. The basic elements of the DOM are the optical sensor for Cherenkov light, an electronic circuit board for processing signals, a HV generator for the optical sensor, an optical beacon for calibration purposes, and the glass pressure housing.

Below are summary of elements in DOM other than PMTs.

Analog Transient Waveform Digitizer (ATWD) In the individual DOM, the ATWD convert

5

analog signal of PMT into digital. Sampling rate is 500 MHz.

Resisting pressure glass To withstand pressure because PMTs are buried deep down in the bowels of the earth.

Geomagnetic shield To paralyze geomagnetic influence.

Optical gel To hold on the PMT.

Flasher board To use position measurement of individual PMT and measurement of glacial degree of clearness

Electronics board To supply high voltage to PMT. etc

10 inches PMT for the IceCube

Figure 1.3: Left:DOM (Digital Optical Module) individual parts. Right:PMT.

The optical sensor is a medium size, which is 10 inch diameter, hemispherical photomultiplier tube (PMT), R7081-01, with 10 dynodes inside, made by Hamamatsu. PMTs very similar to the intended device have been deployed within AMANDA, which the sensor size of is 8 inch diameter, with generally excellent experiment. These large PMTs offer surprisingly good time resolution, as indicated by a Transit Time Spread (TTS) for Single PhotoElectron (SPE) pulses of about 2.5 ns RMS. Photo cathode sensitivity extends well into the ultraviolet rays (UV), limited by the optical transmission of the glass pressure sphere at 350 nm. However, this PMT has not flat, but the spherical photo cathode to enlarge the collection area and has designed to reduce the time difference of photoelectrons coming from different points of the surface to

the dynode. Generally, the sensitivity of the photo cathode is not uniform, especially in case of large PMTs. A PMT collects individual photoelectrons from the surface of the PMT to the dynode by inducing electric field inside the PMT. The configuration of the electric field is determined by the dynode arrangement whose adjustment requires careful special technique. Therefore, the shape of the spherical surface is likely to have difference individual PMT. The costing on the inner surface of photo-cathode is also likely to be not perfectly uniform.

Chapter 2

Calibration of the PMT at the freezing temperature

The IceCube experiment equips the PMT in Digital Optical Module (DOMs) at Atlantic ice. Careful measurement needs to be made to confirm whether the PMTs work properly in operation. Results of measurement is also used in DOM Monte Carlo simulation and event reconstruction program. Our calibration program mainly constitutes following items.

1. SPE (Single Photo-Electron) response Measurement

2. Noise rate counting

3. Wave form taking

2.1 SPE response Measurement

PMT response is linear to number of photo-electrons unless saturation occurs. A study of SPE response is, therefore, fundamental to understand DOM behavior.

2.1.1 Introduction

The present measurement uses Analog to Digital Converter (ADC), that is the device to integral electric pulse and digitize. Incoming photon hitting the photo-cathode surface of the PMT

8

generates photo-electrons, which are amplified by the dynodes with 10 stage, resulting in detectable current. This current is converted to voltage pulses by introducing proper impedance. PMT gain is calculated from the charge of SPE signal which can be estimated by area of a pulse processed by ADC.
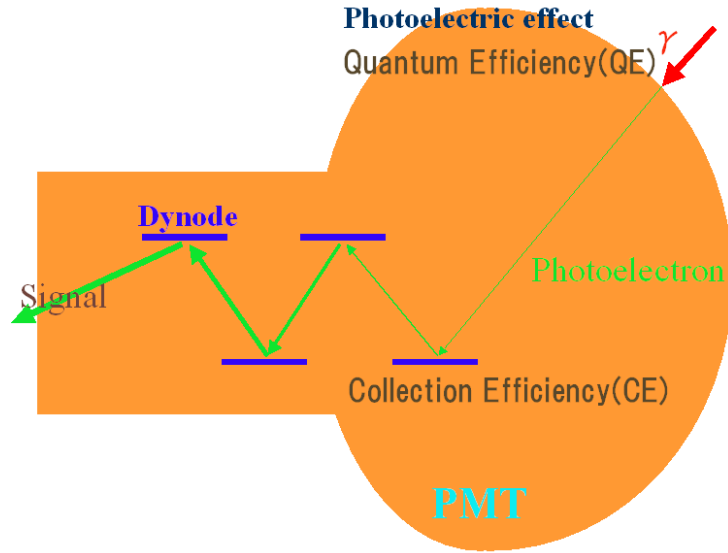
Figure 2.1: Amplification of photo-electron in the PMT

This gives

$$Gain = \frac{\overbrace{q0}^{SPE - ped} \times \overbrace{0.25 \times 10^{-9}}^{1\ bin\ of\ ADC\ =\ 0.25pC}}{\underbrace{1.604 \times 10^{-19}}_{1C}} \qquad (2.1)$$

Amplified electric charge is subject to statistical fluctuation, which, in principle, follows Gaussian. Its peak gives PMT Gain and its width corresponds to charge resolution.

The IceCube collaboration has determined criteria of PMTs for stable operation and securing physics targets. The criteria are:

- Gain $\geq 5 \times 10^7$ for HV $\leq$ 2000[V].

- P / V $\geq$ 2.0

- Dark current (noise rate) $\leq$ 1 [kHz] Targeted number : 500 [Hz]

9

2.1.2 Measurement Setup

Cooling down PMTs are realized by putting them into the Freezer shown in Figure 2.2) . The temperature is set to -32 C°, which PMTs are expected to experience at the IceCube instrumented volume. The cooling process takes 8 hours before starting the measurement.

Figure 2.2: Freezer

The data-taking uses electric modules described in Table 2.1.
The procedure of SPE data-taking is as follows.

1. Configure the modules as shown in Figure 2.3. Intensity of Light source is set as 0.2 photon / shot. So that probability of more than 2 photon / shot is negligible. A gate for ADC trigger is provided by sync signals of the function generator. It width is set as 70 ns by the gate generator.

2. Light of UV LED uniformly illuminate the forehand surface of the PMT by attaching diffuser as shown in Figure 2.4.

    PMT is attached to divider circuit which provides HV (SHV) and output PMT signal (BNC). This divider circuit is shown in Figure 2.4, which is originally developed by U-Wisconsin and SSEC.

10

MODULE NAME	MODEL	Vendor	NOTES
Function Generator	33120A	Agilent Technology	
Oscilloscope	TDS2012	Tektronix	2ch, digital storage
ADC(Analog to Digital Converter)	2249A	LeCroy	0.25pC/bin,1024ch
Crate controller	CC/7700	Toyo technica	
Dual gate generator	KN1500	Kaizu Works	
8ch Discriminator	N-TM405	Technoland	
4-hold 1-veto coincidence	470	Kaizu	
Quad high voltage	RPH-22	Repic	
16ch TTL-NIM Level Adopter	KN206	Kaizu Works	
Preset scaler controller	150	Kaizu	
Dual variable delay	330	Kaizu	
Light source	LED	Nichiya	UV [380 nm]

Table 2.1: Using measurement tools
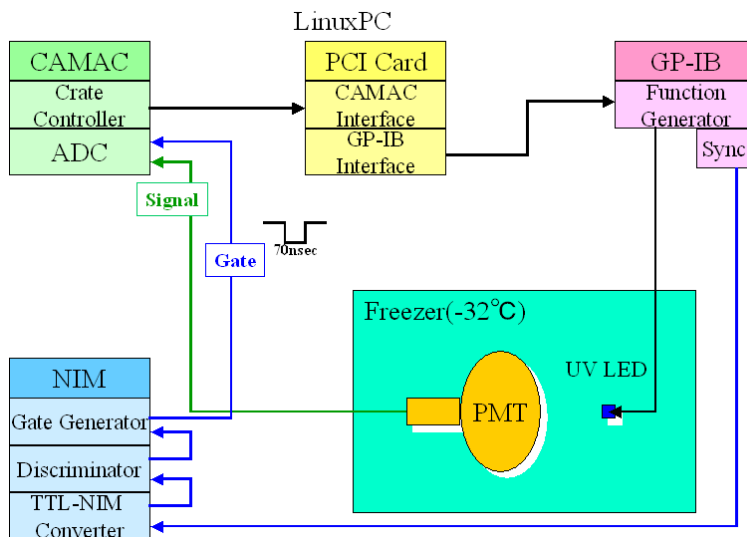
Figure 2.3: Electronics of PMT Gain Measurement

3. At each HV, pedestal run followed by SPE run is carried out. Pedestal run is to take only noise and dark current data without LED illumination. SPE run is to take the data with

Figure 2.4: Left:DOM (Digital Optical Module) individual parts. Right:Divider circuit attaching behind the PMT at Chiba University

LED illumination. Pedestal run histogram has only one peak, while SPE run histogram has 2 peaks, pedestal peak and SPE peak. This SPE run histogram is shown in Figure 2.5.

Figure 2.5: Amplification of photo-electron in the PMT. Gain is 5×10^7 at 1790 [V]. Horizontal axis is ADC count. Vertical axis is number of event.

At first, HV is set to obtain signal pulse hight of approximately $50 \sim 70$ [mV]. Using the fitting program, the gain is calculated. Searching for HV numbers to realize gain of 5×10^7, and 1×10^7, respectively, HV-gain dependence is measured and recorded for individual PMTs.

12

2.1.3 Analysis Procedure: Modeling of SPE response

The Gaussian is found to represent main part of SPE charge histogram, but not the entire part. The non-Gaussian component seems to exhibit exponential-type of function, which is consistent to a possible inefficiency of charge gain at 1st dynode. We found the following function to describe the whole SPE charge response.

$$Q(q, \sigma_0, q_\tau) = \frac{Pe}{q_\tau} e^{-\frac{q-qped}{q_\tau}} + (1 - Pe) \frac{1}{\sqrt{2\pi}\sigma_0 N} e^{-\frac{q-q0}{2\sigma_0^2}} \qquad (2.2)$$

where Pe is ratio of exponent part to all. q_{ped} is ADC count of pedestal peak. σ_0 is σ of SPE part. q0 is difference between ADC count of pedestal peak and ADC count of SPE peak. q0 gives the gain, and σ_0 / q0 gives the charge resolution.
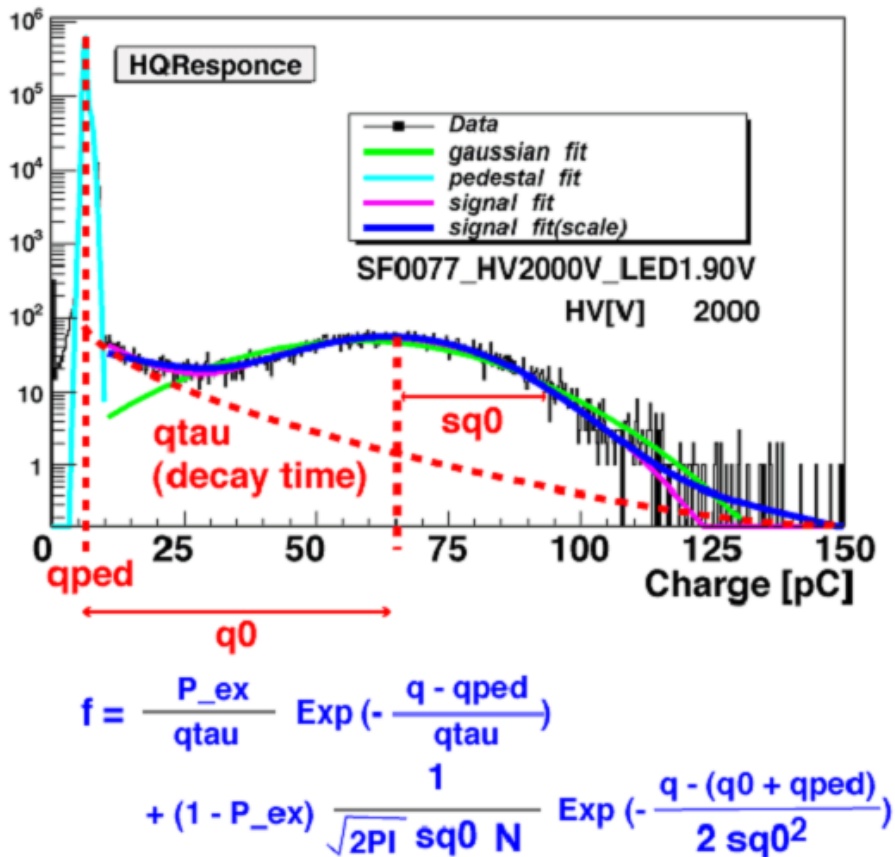
Figure 2.6: PMT model

13

2.1.4 Results

As example pf charge histogram with the fitted model function is shown in Figure 2.7. The gain is calculated to be $5{\times}10^7$. Fitting function well represents ADC distribution. This fitting
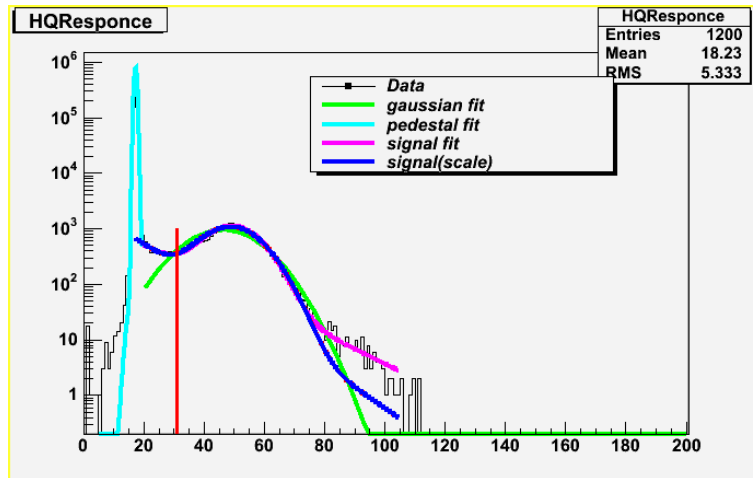
Figure 2.7: ADC spectrum at $5{\times}10^7$. Horizontal axis is ADC count. Vertical axis is number of event.

function can use charge response analysis.

HV dependence of Gain

This dependence is obtained from these PMTs gain data. HV-Gain relation is shown in Figure 2.8.

Compared measurements of Chiba Univ and Hamamatsu

Figure 2.9 shows comparison of HV obtained by Hamamatsu and this measurements. The gain is 5×10^7 in left panel of Figure 2.9, 1×10^7 in right panel of Figure 2.9.

These figure show that gain measured by Chiba this measurements is higher than measured by HAMAMATSU. Gain measurement by HAMAMATSU is based on the PMT current. Light source keep illuminating. Therefore, it is thought that the potential difference is weakened by the scape charge effect, and gain lowers. In addition, the difference of temperatures between Chiba ($-32C°$) and Hamamatsu ($25C°$) would explain this shift.

14
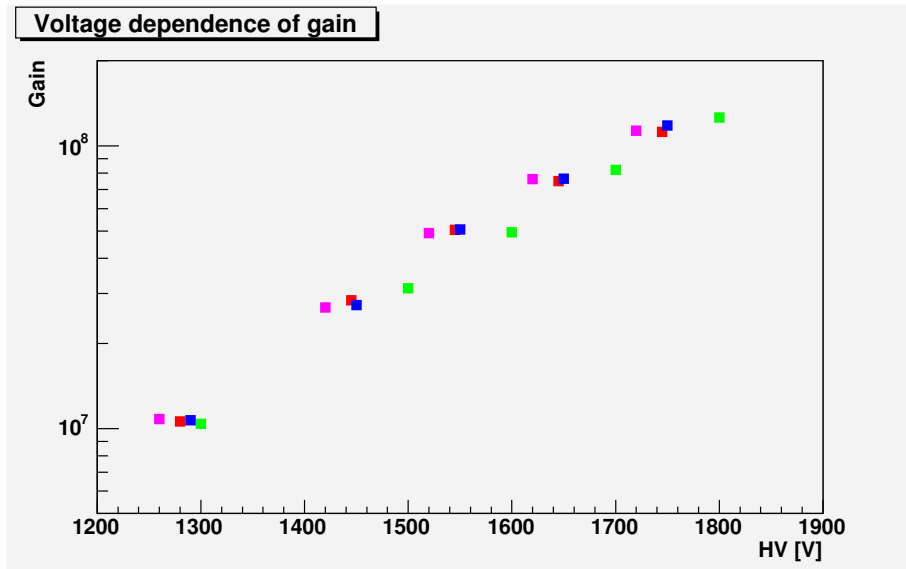
Figure 2.8: HV dependence of gain. Horizontal axis is HV [V]. Vertical axis is gain. Three PMTs marked by different colors are plotted here.
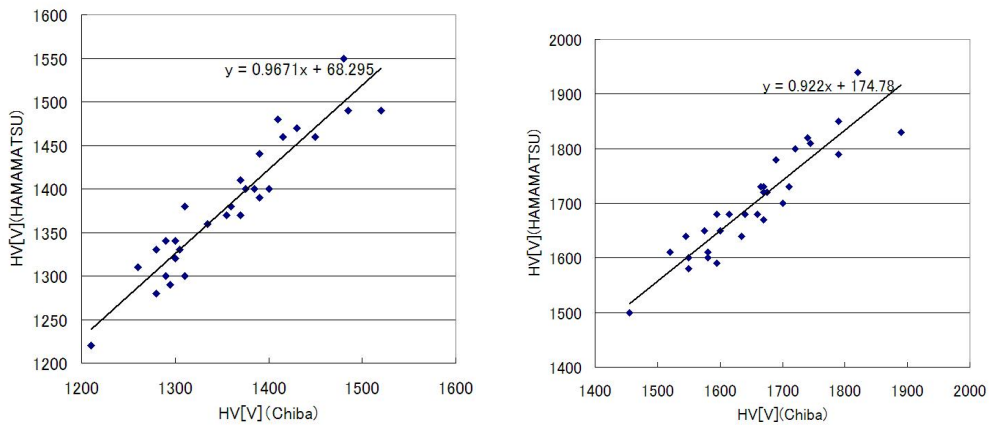
Figure 2.9: Left:Comparison of HV by Hamamatsu and the present measurement at gain of 1×10^7. Vertical axis is measured HV by Hamamatsu, horizontal axis is measured HV by Chiba Univ. Right:Same as left figure, but gain of 5×10^7.
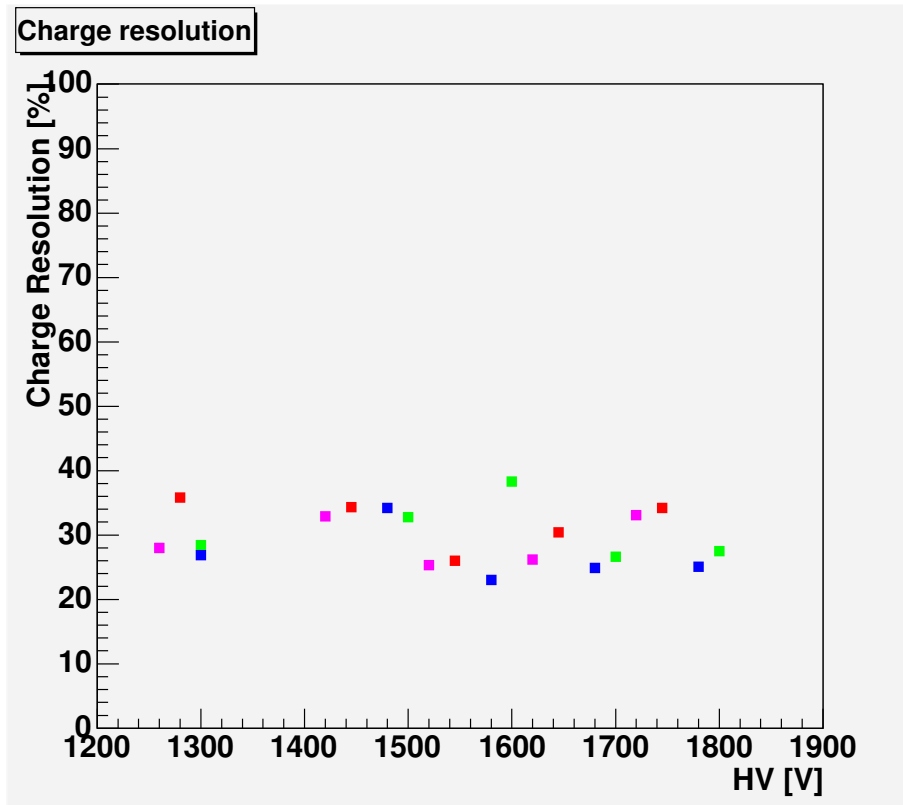
Figure 2.10: Voltage dependence of charge resolution. Horizontal axis is HV [V]. Vertical axis is charge resolution.

HV dependence of Charge resolution

Figure 2.10 shows that charge resolution is not related HV. Charge resolution is almost independent on gain.

Charge resolution distribution at gain of 5×10^7

Charge resolution differs from PMT to PMT, but not much. Shown in Figure 2.11 is distribution for all PMT value at gain of 5×10^7.

HV dependence of Peak to valley ratio

Figure 2.12 shows voltage dependence of peak to valley ratio. As HV is increasing, peak to valley ratio is increasing. This figure shows that the criteria of peak to valley ratio, ≥ 2.0 at
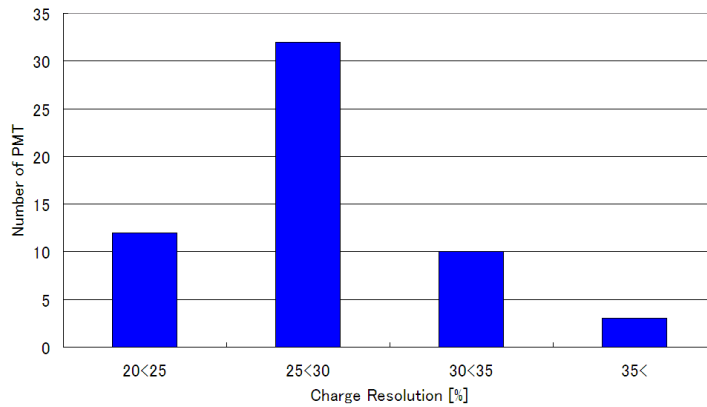
Figure 2.11: Charge resolution distribution uses all PMTs data. Vertical axis is a number of PMT, horizontal axis is charge resolution value

gain of 5×10^7, is satisfied.

Peak to valley ratio distribution at gain of 5×10^7

Figure 2.13 shows that peak to valley ratio distribution for various PMTs at gain of 5×10^7. It is found that all the PMTs satisfied the P / V criteria.

2.2 Noise Rate Measurement of the PMT at low temperature in Freezer

2.2.1 Introduction

In order to suppress trigger rate of the whole detector less than 1 [kHz], noise rate of individual PMT must be less than 500 [Hz], at gain of 1×10^7. The noise (dark count) rate is determined by frequency of pulses exceeding 0.3 p.e. It corresponds to 15 ~ 20 [mV] for PMTs with gain of 1×10^7. Unfortunately this is too low for conventional NIM modular. Here, we measure the rate at gain of 5×10^7 instead. Calibration of the gain dependence of the rate is done later by using wave form data acquired by digital scope.

17
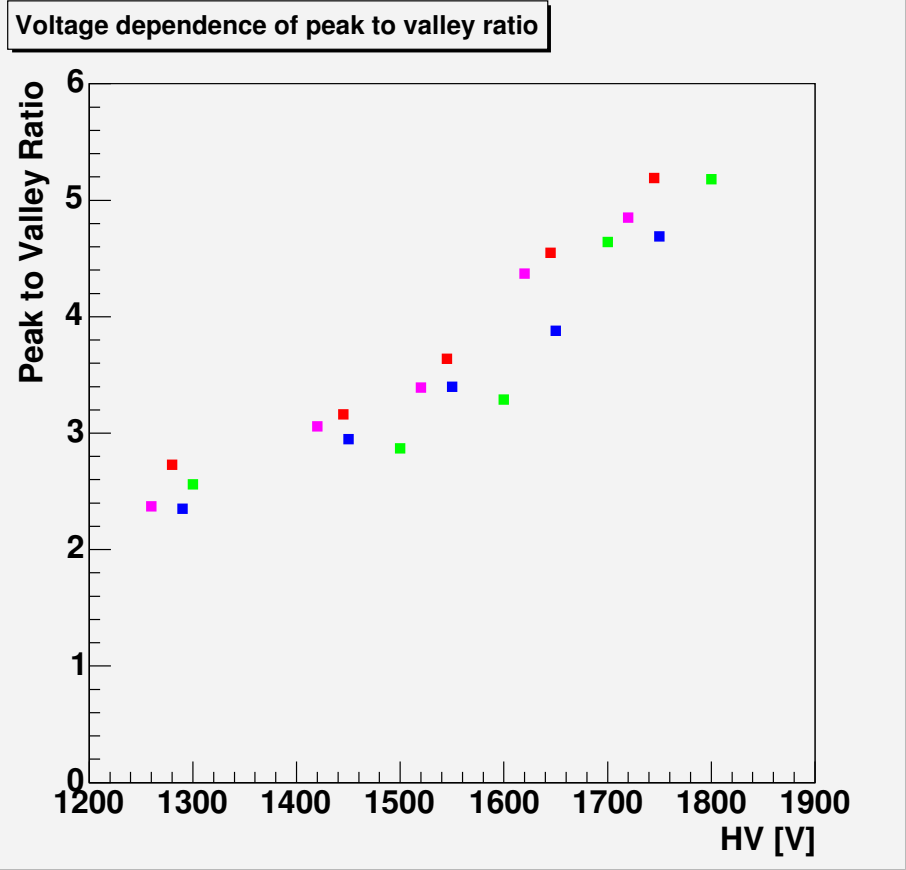
Figure 2.12: This figure is voltage dependence of peak to valley ratio. Horizontal axis is HV [V]. Vertical axis is peak to valley ratio.
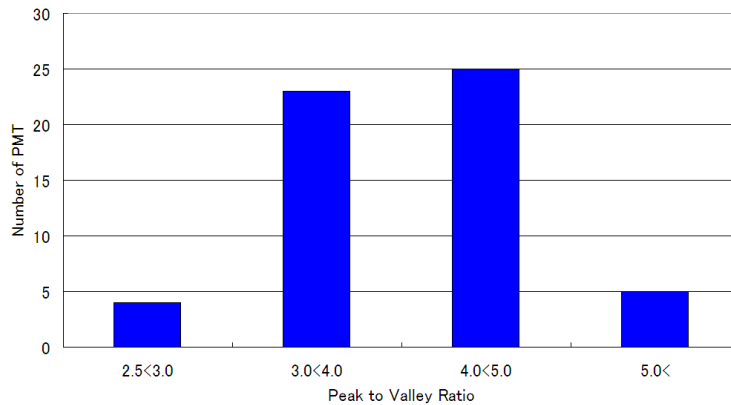
Figure 2.13: Peak to valley ratio distribution uses all PMTs data. Vertical axis is a number of PMT, horizontal axis is peak to valley ratio

2.2.2 The Noise Rate Measurement System

Measurement Setup

NIM discriminator is plugged into signal of the PMT. Threshold is set 0.3 photon by measured average pulse hight of 1 photon.

How to decide threshold of 0.3 p.e.

Measurement of 1.p.e. pulse hight uses digital oscilloscope triggered (Oscilloscope:CH2) by Sync signal (2 kHz) of function generator. Configuration of electric circuits as shown in Figure 2.14 is almost identical to measurement of ADC spectrum.

1. 1000 event of pedestal is taken by the digital oscilloscope. SPE component is taken 20000 event. Because probability of 1 photon detected the PMT is small, SPE signal is contained only in 30~50 [event] / 2000 [shot].

2. In analysis, time width of gate is set 100 ns. Maximal hight of waveform is read out from pedestal data. Determine maximum value among 10000 events. Call this voltage "TrigV".

3. Search for pulses exceeding TrigV in SPE run data. Average of these pulse hight is calculated and called "1peV".

19

4. $0.3 \times 1\text{peV}$ is defined as "0.3peV". This is the level of discriminator.

An example of these numbers are summarized in Table 2.2 for PMT "SF0023".

Gain	HV[V]	TrigV[mV]	1peV[mV]	0.3peV[mV]
5×10^7	1840	8.0	57.97	17.39
1×10^7	1500	1.6	11.33	3.40

Table 2.2: SF0023's TrigV[mV], 1peV[mV] and 0.3peV[mV] at -30 C°
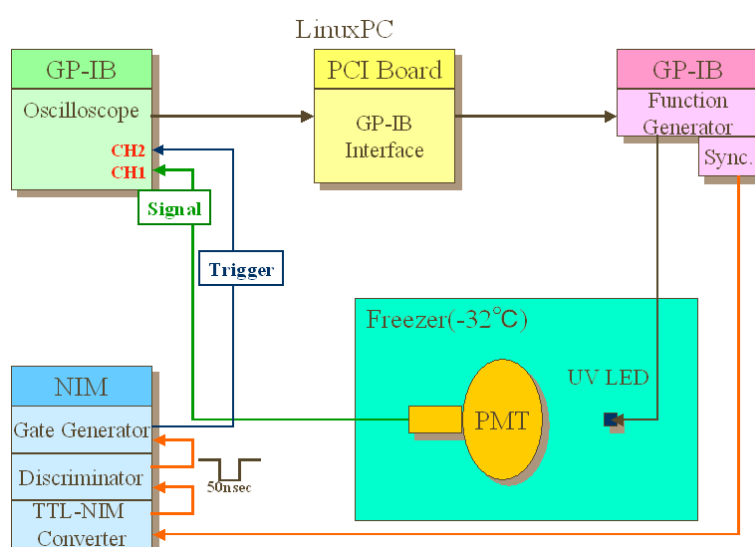
Figure 2.14: Electronics of PMT 1.p.e pulse hight decide Measurement

The procedure of noise rate measurement

1. Plug signal into discriminator with level of "0.3peV". Wire the relevant electronics as illustrated in Figure 2.15.

2. To eliminate the after-pulse effect, wider gate pulse is formed by the gate generator and plugged into the NIM scalar. The gate width is varied from 100 ns to 10 μsec.

3. Output of the gate generator plug into the scalar. Time [s] is measured by scalar until 10000 count, which is count number of scalar.
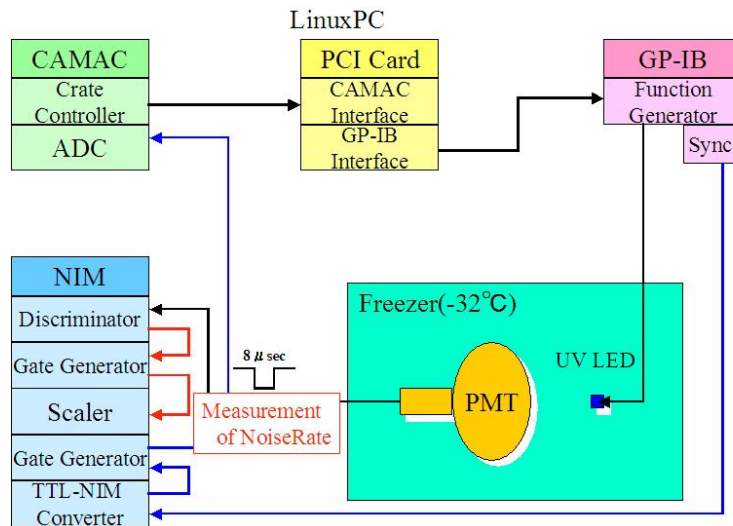
Figure 2.15: Electronics of PMT noise rate Measurement

Analysis Procedure

Analysis method is

$$NoiseRate \ [Hz] \ = \ \frac{10000 \ [event \ number]}{t \ [s]} \tag{2.3}$$

where t is Time [s] measured by scalar. Noise rate is calculated by this method.

Results

In general, the after pulse is expected to be vetoed by 5 μs of gate. A major fraction of PMTs are found in the range of 500 ~ 700 Hz.

2.2.3   Noise Rate Measurement System for lower gain (1×10^7) PMTs

Motivation

If dark noise pulses scaled to the PMT gain, noise rate with threshold of 0.3 p.e. should be independent of PMT gain. This would be the case for thermal noise, other contributions would break this scaling, however. We need to study how much the noise rate charges with the gain and obtain the calibration constant if necessary.
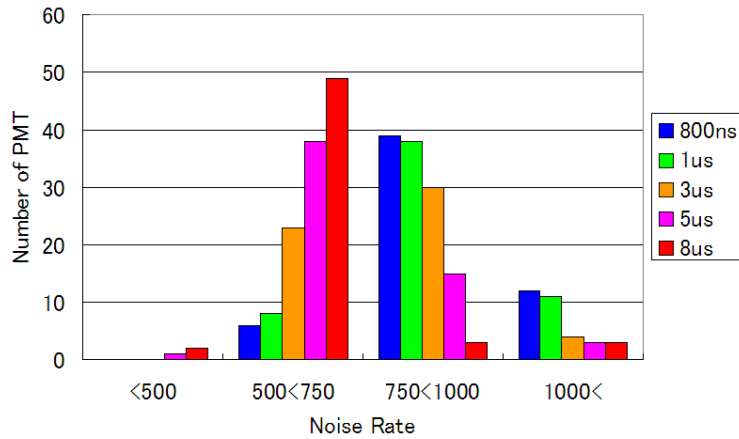
Figure 2.16: Vertical axis is a number of PMT, horizontal axis is noise rate at gain of 5×10^7

Measurement setup

1. NIM Discriminator is plugged into signal of the PMT. Threshold is set for 0.3 p.e. level by measured average pulse hight of 1 photon. Configuration of electric circuits as shown in Figure 2.14 is almost equal to that for measurement of SPE response.

2. Plug signal into the digital oscilloscope (CH1). This trigger uses internal trigger of the digital oscilloscope. This internal trigger is set random.

3. 1 event taken the digital oscilloscope is time width of 10μ[s]. This event is taken 1000 event. Accumulated data acquisition time is 0.1 s.

Analysis Procedure

The analysis program uses software veto for voltage data for given gate time width. This gate width is varied form 500ns to 10μs. Threshold of this program is set voltage of 0.3 p.e..

By using this analysis, these data are compared the noise at gain of 5×10^7 to the noise count at gain of 1×10^7.

Result

Result is shown in Figure 2.3.

Temp	Gain	HV[V]	10μs	3μs	1μs	800ns	500ns
-30	5×10^7	1840	520	590	650	650	660
-30	1×10^7	1500	490	530	580	580	610
-40	5×10^7	1840	580	740	950	1010	1080
-40	1×10^7	1510	490	560	730	750	780
-50	5×10^7	1840	610	690	780	790	790
-50	1×10^7	1490	470	510	540	550	550

Table 2.3: SF0023's noise rate [Hz] of taking oscilloscope

If suggested that the rate weakly depths on the gain, the calibration factor is obtained by

$$average\ ratio(Noise\ Rate\ of\ 1{\times}10^7/Noise\ Rate\ of\ 5{\times}10^7)\ =\ 0.774 \pm 0.118 \quad (2.4)$$

This formula indicates that noise rate specification, 500 [Hz] for gain of 1×10^7, corresponds to 646 ± 110 [Hz] at gain of 5×10^7. Failure rate for all 58 PMTs we measured is 29 %.

2.3 Waveform Taking of the PMT at low temperature in Freezer

2.3.1 Introduction

Analog Transient Waveform Digitizer(ATWC) used by the IceCube can record waveform like FADC. Time width of the ATWC is ~3ns. SPE pulse width and width error needs to be measured.

2.3.2 Measurement Setup

1. Signal component from the PMT in the freezer is divided into two parts. One goes to data taking component and another to the trigger module. Signal component plugs into CH1 of the oscilloscope which records time and voltage. Trigger component plugs into the discriminator device, which is set 10 mV of threshold. This threshold value should

have been to set 8.7 mV, which is half voltage of 0.3.p.e pulse hight at $5{\times}10^7$. But this can not be realized because it is lower than minimum value of the discriminator device threshold. Both this output of the discriminator and sync signal of the function generator plug into the coincidence device. CH2 of the oscilloscope is plugged into output of the coincidence device. The oscilloscope takes pulses only exceeding 10 mV, approximately 0.4 p.e. level. Note the pulse hight of SPE becomes half, since signal component is divided into two parts. This electronics circuit is shown in Figure 2.17.
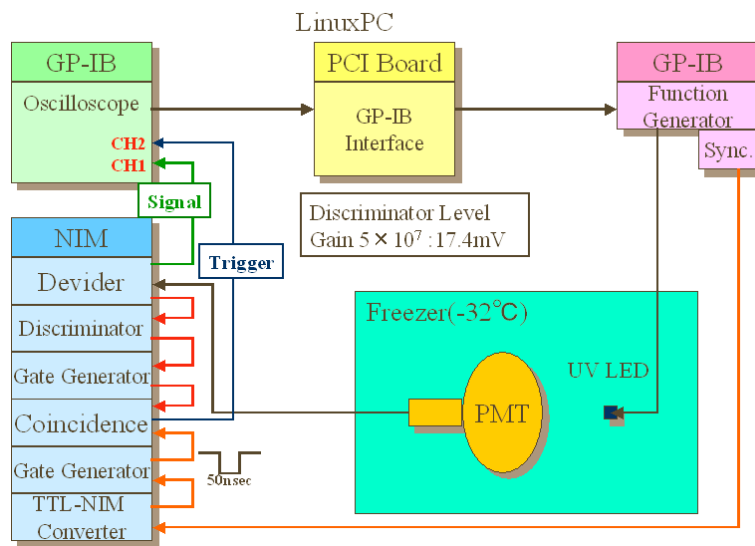
Figure 2.17: Electronics of PMT Waveform Measurement

2. Wave form data, included time and voltage, is taken 1000 event by the oscilloscope.

2.3.3 Analysis Procedure

1. Taken data of 1000 event one by one is fitted by the waveform function. This function is

$$f \;=\; \underbrace{-\frac{n}{\sqrt{2\pi}\sigma}e^{\frac{(-((x-p)^2)}{2\sigma^2)}}}_{Gaussian\ Function} + \underbrace{ground}_{mean\ of\ front\ pulse\ before\ SPE\ signal} \tag{2.5}$$

where σ is the pulse time width, n is normalization factor, p is peak time of the 1.p.e signal and ground is ground level. This function is taken the fluctuation of ground into account Gaussian component. An example is shown in Figure 2.18, which is obtained

24

from average 1000 events. Ground is estimated by taking signal mean before the start of SPE pulse. The fitting procedure is described as follows.

- SPE pulse peak is searched.

- Fit the pulse around 2 ns of the peak by the Gaussian function.

- σ and Peak of the parameter calculated from this fit are put as an initial value of the Gaussian function. And ground value is substituted. Entire SPE pulse including 3 σ area the peak is then fitted by the Gaussian function in the width of 3 σ.
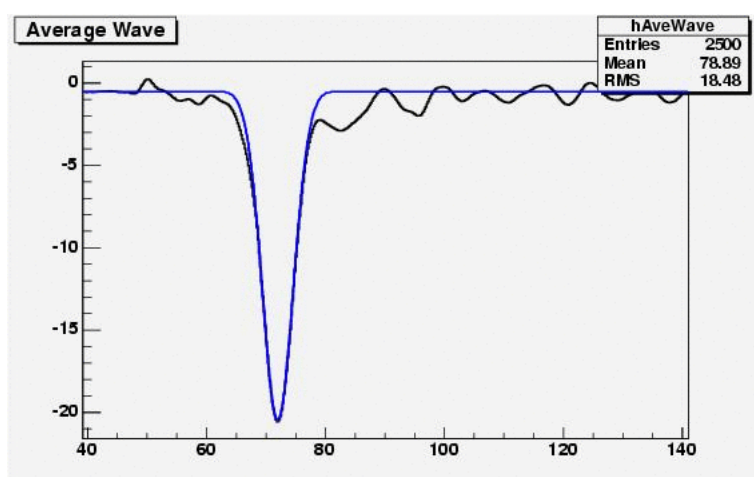
Figure 2.18: TA0352 Waveform of 1000 event total. Black line is measurement data. Blue line is fitting. vertical axis:voltage[mV] horizontal axis:time[ns]

2. Converting digital counts to voltage and time. Time width and error of waveform is calculated.

2.3.4 Result

Half of single pulse width is 1.8 to 2.4 [ns]. This pulse width error is 6 to 14 % . Because ATWD's sampling time width is 2 [ns], the pulse width error do not need to take into consideration. This half of SPE pulse width distribution is shown in Figure 2.19 for all PMTs at gain of 5×10^7.
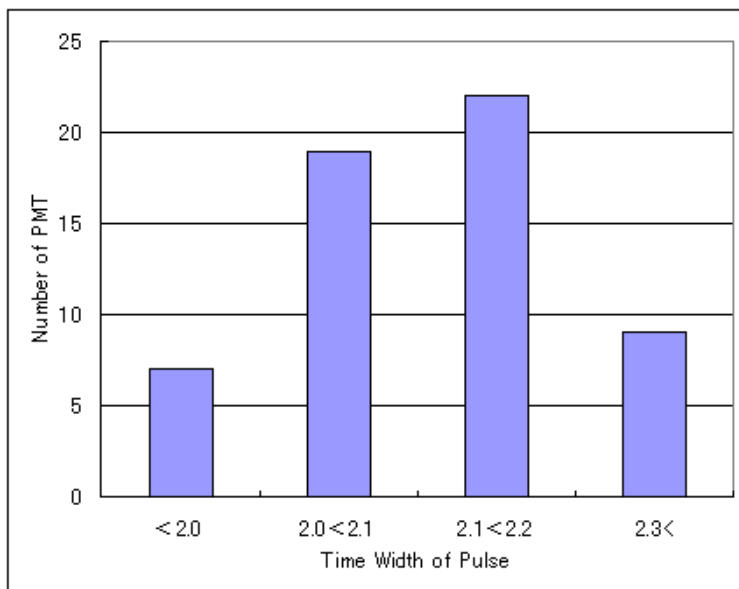
Figure 2.19: Half of SPE pulse width distribution uses all PMTs data. Vertical axis is a number of PMT, horizontal axis is time width of SPE pulse at gain of 5×10^7

Chapter 3

ROMEO (the Root-based Optical Module EmulatOr)

3.1 What is ROMEO?

In order to reconstruct actual events observed by the IceCube, all the results obtained in the present PMT measurements must be simulated in the detector Monte Carlo module. ROMEO simulator utilizing the ROOT TTask function has been developed by the Chiba IceCube group.

ROMEO simulates the photon propagation inside the DOM sphere and the PMT response using our analytical model describing our PMT calibration data. The simulator mainly consists of two packages. First package is responsible for photon propagation inside the DOM while second one takes care of the PMT response. The PMT response package consists of several TTask modules to calculate photo-electron conversion, charge response and waveform of PMT signals.

3.1.1 glass gel module simulation section

The glass transmittance and photon detection efficiency depends on wave length. The Cherenkov spectrum, $\sim \lambda^{-2}$, determines the wave length spectrum DOM would see, propagation of photons in ice modify the spectrum, however. We ran MC simulation to propagate a bulk of photons in ice and built the analytical model.

Using this analytical model, wave length of individual photon is estimated and assigned.
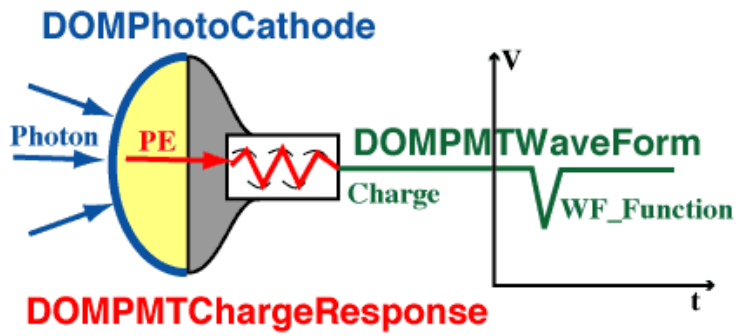
Figure 3.1: ROMEO simulator picture.

The transmittance of the photon path from glass to gel to PMT surface has been calculated by GEANT4-based simulation and its numerical results are implemented by ROMEO to take care of the photon propagation.

3.1.2 charge response of PMT surface(2D gain and collection efficiency) section

This part of modules in ROMEO simulates the PMT response. For a photon hitting the photo-cathode surface, it determines whether it is converted to photo-electrons or not by taking into account the 2D scan of PMTs made by Chiba IceCube Group. A converted photo-electron generates charge and a pulse of waveform following the calibration results described in the previous chapter.

3.2 Study of DOM average response

First average response of DOM to multiple photons is investigated. A photon beam of $10^4 \gamma$s illuminates DOM in the ROMEO simulation to obtain the average behavior.

3.2.1 Analysis Procedure

Number of photon emitted from hypothetical Cherenkov light source is set 10^4 photons par event. 1000 events are generated. The light source area is 1 m^2. The light source located at 0

meter and 50 meters from the DOM, respectively, to investigate the efficiency dependences on the Cherenkov wave length spectrum after propagation. In fact, DOM to DOM distance is 125 meters and this distance is moderate. This Cherenkov light assumes to form parallel beam. The place of the light source is moving by 5 ° around the DOM. from -135 ° to 135 ° where 0 ° is defined as vertical to DOM, as illustrated in Figure 3.2.
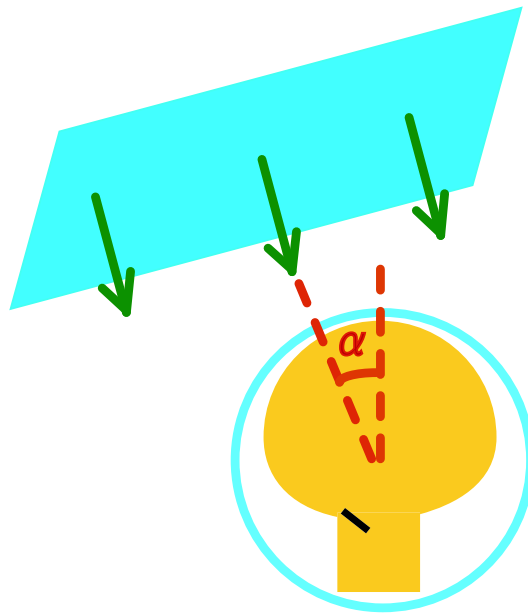
Figure 3.2: This figure is $\alpha°$ of the light source angle.

Figure 3.2.1 shows that acceptance ratio of photons is about 6 % in front of the DOM. Black board in these figures is the first dynode. When angle is negative value, direction of photon's travel is head off to the first dynode.

This figure's red line is Gaussian fit. Red line's sigma parameter is statistical error.

3.2.2   Result

Figure 3.4 shows that number of detected photo-electrons for incoming $10^4\gamma$s as a function of beam angle. It corresponds to DOM "acceptance" for photon detection. A little asymmetry is found in this acceptance curve. It is understood that the sensitivity of the detector depends in the direction of 1st dynode. In order to study PMT to PMT variances, three different PMT data is used in the simulation for comparison. One PMT represents a typical standard behavior of
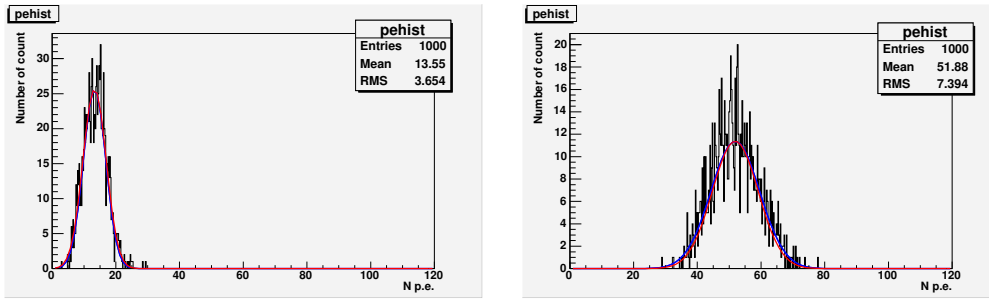
Figure 3.3: Left:Angle of the light source is -90 °. Horizontal axis is number of created photo-electron. Vertical axis is number of count. Right:Angle of the light source is 0 °.

PMTs while other two represents good ones and bad ones in terms of uniformity and charge resolution. Good PMT is consistent of standard PMT. But bad PMT is not consistent. In the angle of sharp, difference of acceptance is about 40%.
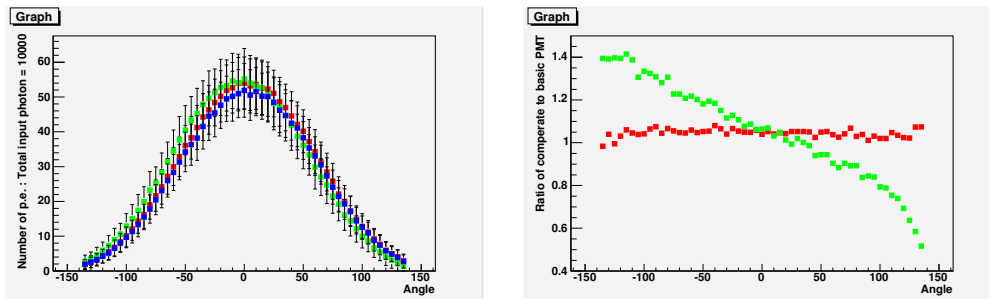
Figure 3.4: Left:Horizontal axis is angle [°], Vertical axis is number of p.e.. Blue point is standard PMT. Red point is a bad PMT. Green point is a good PMT. Right:Horizontal axis is angle [°], Vertical axis is ratio as a standard of the PMT

Figure 3.5 shows dependence of distance to the DOM from the light source. Acceptance of 0m of distance is about 60% of fixing wave length acceptance. Acceptance of 50m of distance is about 45% of fixing wave length acceptance.

Estimate of F value

F value is a value to indicate a factor of fluctuation to the statistical number. α is a value in which it showed charge resolution of the DOM.

$$\mu_{pe} = \bar{N}_{pe} \tag{3.1}$$

30
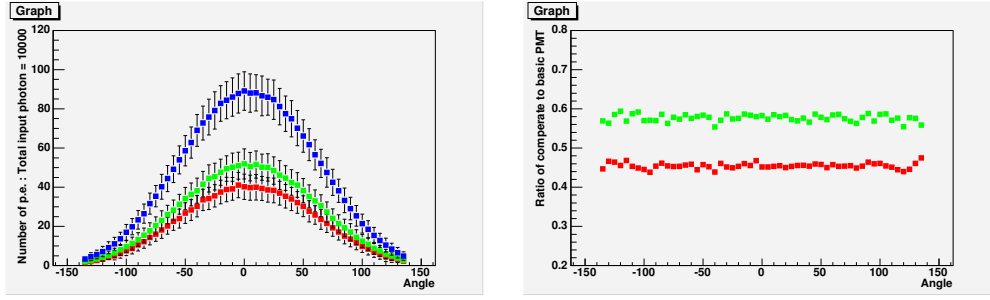
Figure 3.5: Left:Horizontal axis is angle [°], Vertical axis is number of p.e.. Blue point is fixing wave length. Red point is 50m of the light source from the DOM. Green point is 0m. Right:Horizontal axis is angle [°], Vertical axis is ratio as a standard of the fixing wave length.

$$\sigma_{pe}^2 = \bar{N}_{pe} \tag{3.2}$$

$$\bar{N}_{pe}^c = \gamma \bar{N}_{pe} = Q \tag{3.3}$$

$$\tag{3.4}$$

where μ_{pe} is peak of the right figure as shown in Figure 3.7, σ_{pe} is σ took into consideration Poisson assumption. $\bar{N}_{pe}^c$ is peak after gained. γ is excepted value of 1.p.e. distribution. $\gamma = \int f(x)$. $f(x)$ is addition Gaussian turn and exponential turn. This γ factor is ratio of peak in right figure and left figure as shown in Figure 3.6.

$$\sigma_{PMT}^{1pe} = \sigma_{R,Q} \times 1_{pe} \tag{3.5}$$

$$(\sigma_{PMT}^{Npe})^2 = (\sigma_{R,Q}^2 \bar{N}_{pe}^2)/\bar{N}_{pe} \tag{3.6}$$

$$= \alpha^2 \bar{N}_{pe} \tag{3.7}$$

$$\tag{3.8}$$

where $\sigma_{R,Q}$ is charge resolution value, σ_{PMT}^{Npe} is width of addition match of 1.p.e. charge distribution.

$$(\sigma_Q)^2 = (\sigma_{pe}^2 + \sigma_{PMT}^{Npe\ 2})\gamma^2 \tag{3.9}$$

$$\tag{3.10}$$

where σ_Q is estimated value by used σ_{pe} and σ_{PMT}^{Npe} as shown in Figure 3.7.

31

$$\frac{\sigma_Q^{\ 2}}{\mu_{pe}} = (1 + \sigma_{R,Q}^2)\frac{1}{\bar{N}_{pe}} \tag{3.11}$$

$$3\frac{\sigma_Q}{\mu_{pe}} = \sqrt{1 + \sigma_{R,Q}^2}\frac{1}{\sqrt{\bar{N}_{pe}}} \tag{3.12}$$

$$F \equiv \sqrt{1 + \sigma_{R,Q}^2} \geq 1 \tag{3.13}$$

$$\tag{3.14}$$

$\sigma_{R,Q}$ is replaced by α. α is a value of more than $\sigma_{R,Q}$. F value is $\sqrt{1 + \alpha^2}$.
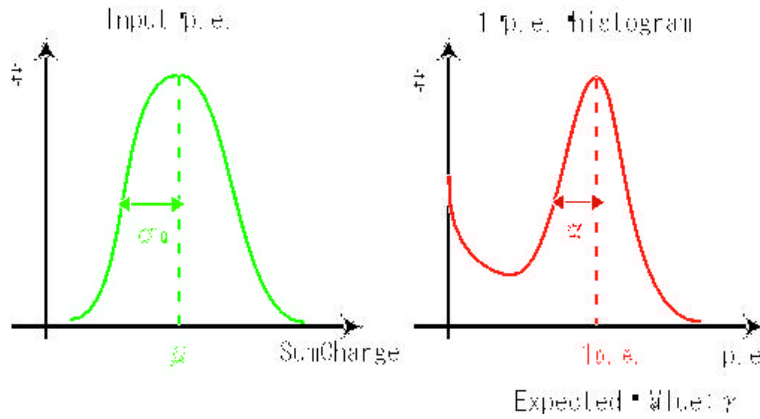
Figure 3.6: Left:Total charge distribution before gain. Horizontal axis is sum charge, Vertical axis is number of count. Right:1 photo-electron charge distribution. Horizontal axis is charge, Vertical axis is number of count.

F value is almost consistent. But F value is inconsistent at point where the angle is sharp.

3.3   Study of DOM response to a single photon

3.3.1   Analysis Procedure

Number of photon emitted hypothetical Cherenkov light source is set 1 photon par 1 event. 10^7 event are generated. This Cherenkov light assumes to form parallel beam. The place of the light source is moving by 5° around the DOM from -135 ° to 135 °, too.

Event of more than 0.3 photo-electron is counted.
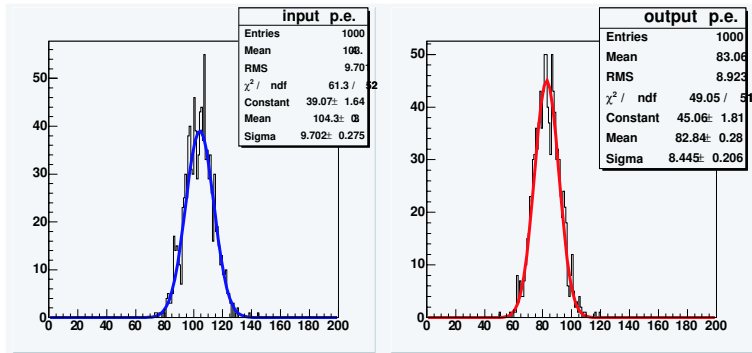
Figure 3.7: Left:Total charge distribution before gain. Horizontal axis is sum charge, Vertical axis is number of count. This blue line is Gaussian fitting. This peak is called μ. This σ is called σ_Q. Right:Total charge distribution after gain. This red line is Gaussian fitting. This peak is $\gamma \times \mu$. This σ is $\gamma \times \sigma_Q$.
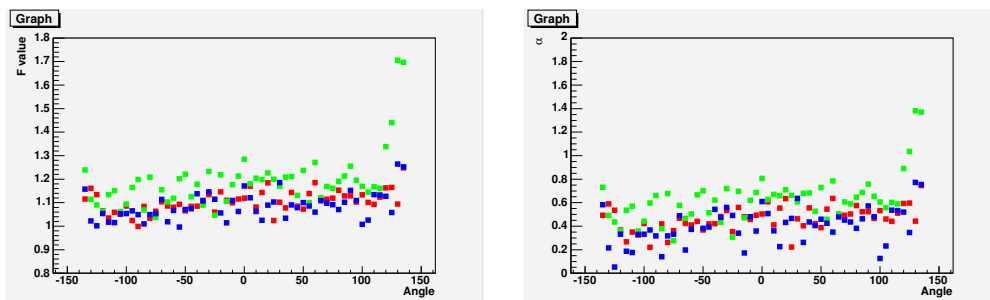
Figure 3.8: Left:Horizontal axis is angle [°], Vertical axis is F value. Blue point is standard PMT. Red point is a bad PMT. Green point is a good PMT. Right:Horizontal axis is angle [°], Vertical axis is α factor.

Figure 3.9 show that acceptance ratio of photons is about 0.6 % in front of the DOM. Black board in these figures is the first dynode. When angle is negative value, direction of photon's travel is head off to the first dynode.
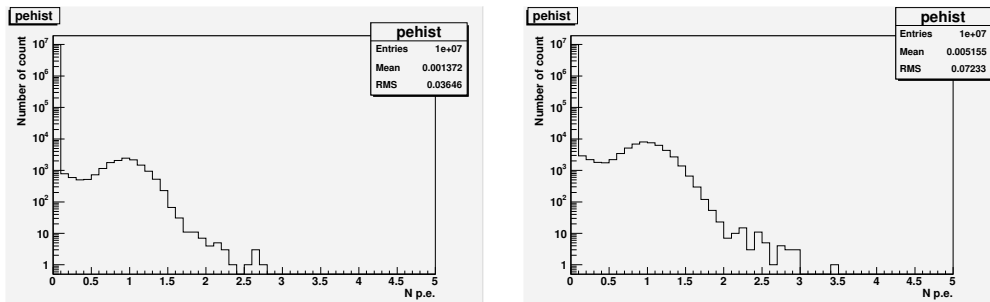
Figure 3.9: Left:Angle of the light source is -90 °. Horizontal axis is number of created photo-electron. Vertical axis is number of count. Right:Angle of the light source is 0 °.

3.3.2 Result

Angle dependence of detected photo-electrons ratio is shown in Figure 3.10. Number of input photon is 1. Good PMT is consistent of standard PMT. But bad PMT is not consistent. In the angle of sharp, difference of acceptance is about 40%.
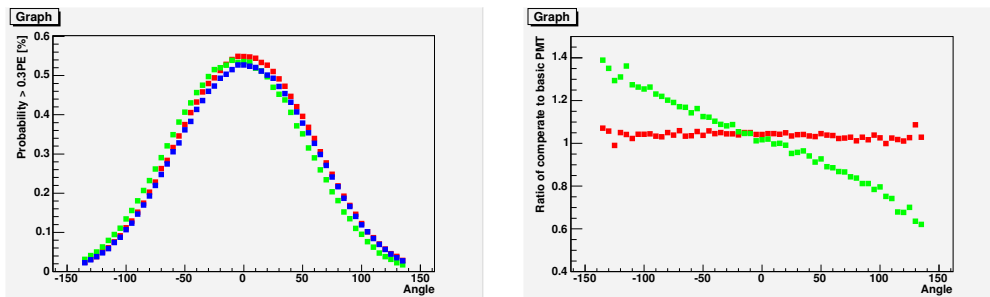
Figure 3.10: Left:Horizontal axis is angle [°], Vertical axis is the ratio of detected event of more than 0.3 photo-electron. Blue point is standard PMT. Red point is a bad PMT. Green point is a good PMT. Distance to the DOM from the light source is 50m. Right:Horizontal axis is angle [°], Vertical axis is ratio as a standard of the PMT.

Figure 3.11 shows dependence of distance to the DOM from the light source. Acceptance

34

of 0m of distance is about 60% of fixing wave length acceptance. Acceptance of 50m of distance is about 45% of fixing wave length acceptance.
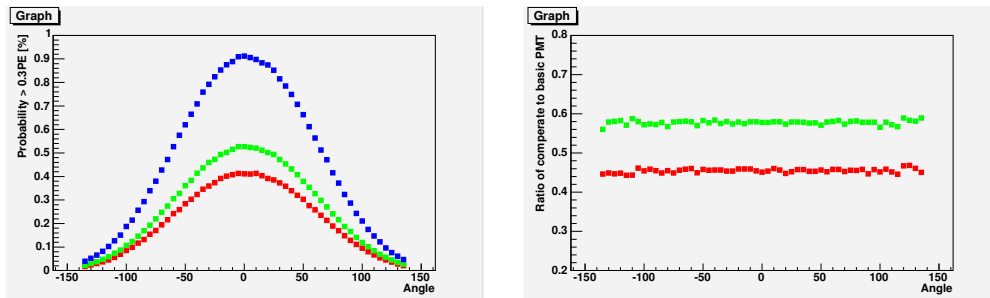
Figure 3.11: Left:Horizontal axis is angle [°], Vertical axis is the ratio of detected event of more than 0.3 photo-electron. Blue point is fixing wave length. Red point is 50m of the light source from the DOM. Green point is 0m. Right:Horizontal axis is angle [°], Vertical axis is ratio as a standard of the fixing wave length.

Figure 3.10 shows detected event ratio of more than 0.3 photo-electron for incoming 1 γ as a function of beam angle. A little asymmetry is found in this acceptance curve. It is understood that the sensitivity of the detector depends in the direction of 1st dynode.

Chapter 4

Summary and Outlook

4.1 Summary

SPE Response

- Modeling of ADC histogram is successful.

- Gain is 1×10^7 less than 2000 [V]. This is satisfied criteria.

- Charge resolution region is 0.21 to 0.41 at 5×10^7.

- Peak to valley ratio is 2.3 to 6.8. This value is satisfied criteria at 5×10^7.

- HV dependence of charge resolution is quite unrelated.

Wave Form Taking

- Modeling of SPE pulse is successful.

- Sigma of SPE pulse is 1.85 to 2.33 [ns]. Specification of ATWD is that sampling time width is 2 [ns]. So, pulse width is no problem.

- SPE pulse width error is 6 to 14 % .

Noise Counting

PMTs are not satisfied noise rate specification. Not satisfied ratio is about 29 %.

All of these data is shown Appendix chapter. **ROMEO simulation**

- Number of output photon-electron depend in the direction of 1st dynode.

- Event ratio of more than threshold depend in the direction of 1st dynode, too.

- Acceptance difference is max 40% at the sharp of angle.

4.2   Outlook

We were able to see the behavior of the PMT almost. The behavior are charge response, noise rate, shape of SPE pulse, 2D gain, 2D collection efficiency and 2D quantum efficiency. We were almost made DOM simulator. As a result, DOM simulator ROMEO is moving by using the parameter of the PMT now. We should do various measurements about the DOM, because we do not understand whether the DOM simulator is suitable for the behavior of the actual DOM. It is necessary to measure the item that method of the DOM measurements is the same as the PMT. It is necessary to judge whether the behavior of the DOM simulator is appropriate by using the result of obtaining from the DOM.

Chapter 5

Appendix

5.1   All data of charge response

These tables as shown in Figure 5.1, Figure 5.2, Figure 5.3, Figure 5.4 and Figure 5.5, are shown all data of charge response measurement.

5.2   Noise rate and Waveform

Noise rate and wave form calibrate data at 5×10^7. This table as shown in 5.6 is all data of measured waveform data and noise rate. Cell painted out that pink is more than 1000 [Hz] of noise rate, yellow's cell is 750 ~ 1000 [Hz], green's is 500 ~ 750 [Hz] and blue's is less than 500 [Hz].

Modelturm	HV	Gain	Error	ChargeRes	Error	PVratio	qtau/q0	pe/q0
TA0348	1955	5.08E+07	2.03E+05	2.87E-01	3.62E-03	4.21	0.51	
TA0348	1958	5.08E+07	2.01E+05	2.81E-01	3.73E-03	4.74		
TA0348	1960	5.19E+07	2.07E+05	2.84E-01	3.68E-03	3.93		
TA0348	1970	5.40E+07	2.46E+05	2.55E-01	4.68E-03	3.25		
TA0349	1675	3.62E+07	1.08E+05	2.40E-01	3.28E-03	1.56		
TA0349	1725	4.45E+07	1.44E+05	2.43E-01	3.40E-03	1.67		
TA0349	1750	4.62E+07	1.24E+05	2.92E-01	2.55E-03	4.05		
TA0349	1775	5.02E+07	1.35E+05	3.08E-01	2.49E-03	4.31		
TA0349	1875	7.55E+07	2.95E+05	2.80E-01	3.68E-03	4.29	0.58	19.03
TA0349	1975	1.08E+08	4.10E+05	2.83E-01	3.56E-03	4.95	0.58	25.15
TA0350	1745	5.04E+07	1.62E+05	2.67E-01	3.06E-03	4.15		
TA0350	1750	5.14E+07	1.78E+05	2.72E-01	3.25E-03	4.34		
TA0352	1520	3.21E+07	5.47E+04	2.34E-01	1.82E-03	3.40		
TA0352	1570	3.97E+07	6.61E+04	2.51E-01	1.70E-03	3.73		
TA0352	1620	4.93E+07	7.94E+04	2.68E-01	1.64E-03	4.17		
TA0352	1720	7.53E+07	1.21E+05	2.81E-01	1.64E-03	4.62	0.74	90.17
TA0352	1820	1.14E+08	1.90E+05	2.85E-01	1.72E-03	5.04	0.72	87.70
TA0356	1850	4.82E+07	2.00E+05	2.88E-01	4.50E-03	4.65		
TA0356	1860	4.92E+07	2.16E+05	3.06E-01	5.10E-03	4.39		
TA0356	1900	5.99E+07	2.19E+05	3.02E-01	4.01E-03	5.00		
TA0357	2050	4.38E+07	1.45E+05	2.63E-01	3.48E-03	4.75		
TA0357	2090	5.02E+07	1.81E+05	2.79E-01	3.33E-03	4.59		
TA0357	2115	5.40E+07	1.76E+05	2.80E-01	3.34E-03	6.08		
TA0523	1590	2.54E+07	3.36E+04	9.17E-02	1.54E-03	1.94		
TA0523	1640	3.21E+07	5.58E+04	2.99E-01	1.49E-03	1.50		
TA0523	1690	5.00E+02	1.07E+06	2.30E+04	2.02E-02	6.00	0.48	2.11
TA0523	1700	5.23E+07	1.08E+06	2.31E-01	2.04E-02	11.33		
TA0523	1710	5.25E+07	8.99E+05	2.85E-01	1.74E-02	5.80		
TA0523	1790	7.34E+07	1.48E+06	2.57E-01	2.14E-02	6.50	0.77	5.26
TA0523	1890	1.13E+08	1.16E+06	2.45E-01	9.70E-03	5.44	0.59	8.77
TA0526	1880	5.00E+07	1.48E+05	2.54E-01	3.00E-03	4.59		
TA0526	1900	5.34E+07	1.55E+05	2.49E-01	2.89E-03	5.21		
TA0528	1950	4.66E+07	2.55E+05	3.45E-01	5.20E-03	3.04		
TA0528	1970	4.99E+07	2.75E+05	3.41E-01	5.25E-03	3.29		
TA0529	1760	5.03E+07	2.23E+05	2.74E-01	4.19E-03	3.66		
TA0529	1780	5.37E+07	1.92E+05	2.84E-01	3.75E-03	2.32		
TA0529	1790	5.53E+07	3.74E+05	2.92E-01	6.36E-03	3.72		
TA0529	1795	5.65E+07	2.94E+05	3.00E-01	4.74E-03	4.23		
TA0529	1800	5.54E+07	5.62E+05	3.45E-01	8.23E-03	2.60		
TA0530	2000	3.40E+07	2.19E+05	2.81E-01	6.47E-03	4.20		
TA0530	2100	4.57E+07	1.94E+05	2.96E-01	4.35E-03	4.36		
TA0530	2115	4.76E+07	1.98E+05	3.05E-01	4.28E-03	4.26		
TA0530	2135	5.02E+07	2.41E+05	3.22E-01	4.81E-03	4.64		
TA0538	1550	3.25E+07	1.68E+05	2.55E-01	5.55E-03	2.78		
TA0538	1600	4.05E+07	2.43E+05	2.46E-01	5.40E-03	4.28		
TA0538	1650	4.92E+07	2.29E+05	2.71E-01	4.52E-03	2.74		
TA0538	1750	7.72E+07	3.73E+05	2.39E-01	4.67E-03	4.87	0.45	15.14
TA0538	1850	1.13E+08	4.99E+05	2.46E-01	4.35E-03	4.56	0.50	19.20
TA0433	1750	4.23E+07	2.55E+05	2.41E-01	5.93E-03	4.74	0.49	14.51
TA0433	1800	5.14E+07	1.55E+05	2.66E-01	2.87E-03	4.50	0.49	31.55
TA0433	1900	7.50E+07	2.56E+05	2.76E-01	3.36E-03	5.59	0.50	37.81
TA0433	2000	1.10E+08	7.68E+05	2.69E-01	7.82E-03	6.45	0.54	20.48

Figure 5.1: Charge response measurement all data vol.1

Modelturm	HV	Gain	Error	ChargeRes	Error	PVratio	qtau/q0	pe/q0
TA0435	1705	3.49E+07	1.73E+05	2.56E-01	4.70E-03	3.88	0.41	19.62
TA0435	1755	4.17E+07	2.09E+05	2.72E-01	4.44E-03	4.46	0.57	10.44
TA0435	1805	5.01E+07	2.56E+05	2.79E-01	4.60E-03	4.78	0.52	15.64
TA0435	1905	7.18E+07	3.85E+05	2.97E-01	4.98E-03	5.32	0.53	23.20
TA0435	2005	1.02E+08	5.83E+05	2.97E-01	3.38E-03	6.67	0.56	27.43
TA0438	1540	3.28E+07	1.76E+05	2.55E-01	5.05E-03	3.27	0.44	11.74
TA0438	1590	4.41E+07	1.82E+05	2.63E-01	3.74E-03	3.64	0.49	10.93
TA0438	1640	4.98E+07	2.07E+05	2.90E-01	4.09E-03	4.97	0.59	22.28
TA0438	1740	7.92E+07	2.87E+05	2.90E-01	3.45E-03	5.47	0.55	32.86
TA0438	1840	1.18E+08	4.08E+05	2.88E-01	3.31E-03	5.22	0.56	40.89
TA0451	1760	3.53E+07	1.46E+05	2.86E-01	3.98E-03	2.88	0.60	28.06
TA0451	1810	4.20E+07	1.52E+05	2.99E-01	3.76E-03	2.98	0.63	34.93
TA0451	1860	4.93E+07	2.03E+05	3.37E-01	4.17E-03	3.32	0.89	38.21
TA0451	1960	7.17E+07	1.96E+05	3.09E-01	2.81E-03	4.19	0.59	77.19
TA0451	2060	9.95E+07	3.71E+05	3.40E-01	3.81E-03	4.05	0.67	61.85
TA0452	1965	3.24E+07	1.04E+05	2.72E-01	3.48E-03	3.27	0.58	32.42
TA0452	2015	3.78E+07	1.29E+05	2.68E-01	3.69E-03	3.67	0.65	16.87
TA0452	2065	4.31E+07	1.39E+05	2.79E-01	3.33E-03	4.23	0.71	23.00
TA0452	2115	4.98E+07	1.62E+05	2.99E-01	3.47E-03	5.19	0.75	25.90
TA0452	2165	5.83E+07	1.48E+05	2.85E-01	2.64E-03	5.29	0.63	52.95
TA0464	1760	3.49E+07	1.72E+05	2.43E-01	4.63E-03	3.49	0.65	2.04
TA0464	1810	4.13E+07	2.83E+05	2.72E-01	6.29E-03	4.52	0.85	0.19
TA0464	1860	4.98E+07	2.31E+05	2.64E-01	4.28E-03	4.78	0.56	1.00
TA0464	1960	7.17E+07	2.65E+05	2.62E-01	3.59E-03	5.84	0.50	2.07
TA0464	2060	1.01E+08	3.30E+05	2.60E-01	3.21E-03	6.37	0.54	28.81
TA0593	1815	3.55E+07	1.55E+05	3.04E-01	4.12E-03	2.40	0.69	46.32
TA0593	1865	4.20E+07	1.59E+05	3.29E-01	2.36E-03	2.57	0.71	66.58
TA0593	1915	4.94E+07	1.67E+05	3.43E-01	3.35E-03	3.01	0.69	82.72
TA0593	2015	6.83E+07	2.57E+05	3.72E-01	3.73E-03	3.35	0.77	85.46
TA0593	2115	9.34E+07	3.41E+05	3.88E-01	3.66E-03	3.76	0.80	94.98
TA0594	1795	3.55E+07	4.53E+05	2.81E-01	1.14E-02	3.89	0.51	6.56
TA0594	1845	4.18E+07	3.39E+05	3.01E-01	7.46E-03	3.40	0.48	21.04
TA0594	1895	4.99E+07	1.89E+05	3.25E-01	3.71E-03	3.82	0.75	40.93
TA0594	1995	6.92E+07	2.56E+05	3.47E-01	3.66E-03	4.48	0.72	51.53
TA0594	2095	9.66E+07	3.39E+05	3.48E-01	3.55E-03	4.55	0.70	58.17
TA0595	1760	3.50E+07	9.87E+04	2.64E-01	2.95E-03	2.93	0.60	42.30
TA0595	1810	4.09E+07	1.26E+05	2.96E-01	3.16E-03	3.22	0.77	39.99
TA0595	1860	4.93E+07	1.45E+05	3.13E-01	3.07E-03	3.37	0.75	54.79
TA0595	1960	6.97E+07	1.88E+05	3.37E-01	2.85E-03	4.28	0.75	67.89
TA0595	2060	9.76E+07	2.65E+05	3.42E-01	2.88E-03	4.61	0.79	73.41
TA0596	1600	3.33E+07	9.64E+04	2.27E-01	2.27E-01	3.53	0.42	25.72
TA0596	1650	4.09E+07	1.32E+05	2.48E-01	2.94E-03	3.54	0.45	30.72
TA0596	1700	5.02E+07	1.53E+05	2.61E-01	2.82E-03	4.20	0.42	39.45
TA0596	1800	7.56E+07	2.18E+05	2.74E-01	2.79E-03	4.65	0.48	46.63
TA0596	1900	1.13E+08	3.59E+05	2.61E-01	2.96E-03	5.14	0.54	44.22
TA0597	1610	3.43E+07	1.16E+05	2.27E-01	3.39E-03	3.16	0.40	9.65
TA0597	1660	4.12E+07	1.29E+05	2.48E-01	2.90E-03	3.92	0.49	14.65
TA0597	1710	5.01E+07	1.69E+05	2.57E-01	3.09E-03	4.83	0.50	21.98
TA0597	1810	7.42E+07	2.35E+05	2.77E-01	3.04E-03	4.86	0.52	36.17
TA0597	1910	1.09E+08	3.33E+05	2.76E-01	2.95E-03	5.41	0.56	43.52

Figure 5.2: Charge response measurement all data vol.2

Modelturm	HV	Gain	Error	ChargeRes	Error	PVratio	qtau/q0	pe/q0
TA0598	1580	3.32E+07	1.42E+05	2.36E-01	4.59E-03	4.63	0.44	4.06
TA0598	1630	4.14E+07	1.49E+05	2.44E-01	3.80E-03	4.64	0.47	6.09
TA0598	1680	5.04E+07	1.80E+05	2.55E-01	3.65E-03	5.01	0.53	17.29
TA0598	1780	7.52E+07	3.13E+05	2.71E-01	4.42E-03	8.00	0.61	22.47
TA0598	1880	1.13E+08	3.90E+05	2.66E-01	3.80E-03	6.10	0.62	32.61
TA0664	1350	1.16E+07	2.60E+05	2.56E-01	1.41E-02	2.30	0.36	9.74
TA0664	1535	2.91E+07	2.20E+05	3.50E-01	5.53E-03	2.78	0.12	30.23
TA0664	1635	4.98E+07	1.96E+05	2.35E-01	4.04E-03	3.52	0.41	24.33
TA0664	1680	6.17E+07	2.02E+05	2.35E-01	3.38E-03	3.93	0.45	36.69
TA0664	1735	7.56E+07	2.68E+05	2.06E-01	8.81E-03	4.08	0.47	39.08
TA0665	1610	2.29E+07	1.89E+05	3.29E-01	6.84E-03	1.77	0.33	3.68
TA0665	1680	3.37E+07	1.56E+05	2.38E-01	4.85E-03	3.95	0.38	5.40
TA0665	1780	4.98E+07	2.50E+05	2.58E-01	4.74E-03	4.50	0.46	10.03
TA0665	1880	7.32E+07	3.55E+05	2.58E-01	4.65E-03	5.89	0.50	17.45
TA0665	1980	1.06E+08	5.42E+05	2.65E-01	5.16E-03	6.00	0.55	22.22
TA0666	1660	2.63E+07	3.25E+05	2.14E-01	1.21E-02	2.40	0.45	10.18
TA0666	1835	4.85E+07	9.86E+05	2.85E-01	2.11E-02	5.29	0.60	22.28
TA0666	1935	7.21E+07	9.37E+05	2.30E-01	1.34E-02	6.83	0.75	8.98
TA0666	2035	1.01E+08	1.75E+06	2.66E-01	1.97E-02	6.83	1.13	10.14
TA0772	1280	1.10E+07	1.50E+06	2.70E-01	7.01E-02	1.27	0.30	19.00
TA0772	1550	5.03E+07	1.69E+05	2.56E-01	3.36E-03	3.13	0.41	44.50
TA0772	1650	7.71E+07	3.16E+05	2.79E-01	4.20E-03	3.69	0.44	39.32
TA0772	1750	1.19E+08	5.17E+05	2.88E-01	4.69E-03	4.92	0.45	41.38
TA0773	1310	9.96E+06	9.38E+04	2.97E-01	8.59E-03	1.88	0.73	3.82
TA0773	1495	2.78E+07	3.06E+05	3.40E-01	8.38E-03	2.78	0.18	1.77
TA0773	1595	4.98E+07	2.59E+05	2.08E-01	5.23E-03	3.34	0.41	4.88
TA0773	1695	7.45E+07	4.49E+05	2.64E-01	5.55E-03	4.58	0.22	32.99
TA0773	1795	1.08E+08	5.35E+05	2.95E-01	4.70E-03	5.92	0.13	43.83
TA0774	1450	9.73E+06	4.04E+05	3.31E-01	2.66E-02	1.81	0.46	14.59
TA0774	1690	3.07E+07	4.91E+05	3.43E-01	1.25E-02	2.85	0.31	34.40
TA0774	1790	4.96E+07	2.46E+05	2.55E-01	4.83E-03	2.83	0.45	40.77
TA0774	1890	7.03E+07	4.13E+05	2.62E-01	6.69E-03	4.00	0.37	39.59
TA0774	1990	9.46E+07	7.43E+05	3.12E-01	6.30E-03	5.76	0.22	31.97
TA0781	1360	1.02E+07	7.76E+04	2.71E-01	6.10E-03	2.52	0.38	10.03
TA0781	1560	3.02E+07	1.53E+05	3.00E-01	4.65E-03	2.99	0.40	26.45
TA0781	1660	5.06E+07	1.83E+05	2.22E-01	3.38E-03	4.82	0.42	23.44
TA0781	1760	7.53E+07	2.99E+05	2.37E-01	4.36E-03	6.65	0.41	32.89
TA0781	1860	1.10E+08	2.91E+05	2.40E-01	2.56E-03	6.22	0.49	45.60
TA0898	1520	1.05E+07	1.10E+05	3.53E-01	9.64E-03	1.50	0.71	19.66
TA0898	1790	3.50E+07	3.53E+05	3.36E-01	7.82E-03	2.56	0.34	37.06
TA0898	1890	4.99E+07	2.75E+05	2.89E-01	5.23E-03	2.80	0.43	33.51
TA0898	1990	6.84E+07	4.91E+05	3.27E-01	5.55E-03	3.89	0.15	32.40
TA0898	2090	9.36E+07	4.83E+05	3.18E-01	5.21E-03	3.84	0.53	40.06
TA0901	1355	1.08E+07	5.75E+04	3.41E-01	4.97E-03	2.27	0.06	25.99
TA0901	1540	2.98E+07	2.22E+05	3.51E-01	6.59E-03	2.82	0.52	34.94
TA0901	1640	5.07E+07	2.15E+05	2.68E-01	4.42E-03	4.46	0.47	33.43
TA0901	1740	7.62E+07	3.32E+05	2.73E-01	4.62E-03	4.17	0.52	33.01
TA0901	1840	1.09E+08	6.29E+05	3.12E-01	5.00E-03	5.50	0.20	34.84
TA0902	1335	1.06E+07	2.48E+05	3.17E-01	1.64E-02	2.00	0.52	16.63
TA0902	1515	2.82E+07	2.36E+05	3.57E-01	6.78E-03	3.36	0.63	27.44
TA0902	1615	4.98E+07	1.67E+05	2.53E-01	3.47E-03	4.24	0.45	32.48
TA0902	1715	7.53E+07	2.43E+05	2.63E-01	3.38E-03	4.98	0.53	34.97
TA0907	1295	1.03E+07	2.08E+05	2.47E-01	1.22E-02	1.74	0.33	24.33
TA0907	1480	2.60E+07	1.20E+05	3.29E-01	4.22E-03	3.02	0.56	47.45
TA0907	1580	5.04E+07	1.33E+05	2.28E-01	2.67E-03	4.04	0.45	44.78
TA0907	1680	7.69E+07	1.90E+05	2.41E-01	2.41E-03	4.50	0.48	47.70
TA0907	1780	1.16E+08	3.18E+05	2.51E-01	2.71E-03	4.87	0.51	49.87
TA0908	1370	1.01E+07	1.02E+05	3.42E-01	8.14E-03	2.45	0.60	18.70
TA0908	1570	2.98E+07	1.77E+05	3.61E-01	4.74E-03	3.55	0.11	39.49
TA0908	1670	4.92E+07	3.66E+05	3.12E-01	6.56E-03	3.85	0.11	34.96
TA0908	1770	7.51E+07	3.47E+05	2.89E-01	4.25E-03	5.85	0.17	36.52
TA0908	1870	1.08E+08	5.47E+05	3.16E-01	4.54E-03	5.75	0.17	34.43

41

Figure 5.3: Charge response measurement all data vol.3

Modelturm	HV	Gain	Error	ChargeRes	Error	PVratio	qtau/q0	pe/q0
TA0909	1210	1.04E+07	1.12E+05	2.97E−01	1.03E−02	1.52	0.93	6.58
TA0909	1355	2.59E+07	1.85E+05	3.27E−01	6.49E−03	3.33	0.51	23.34
TA0909	1455	4.98E+07	1.92E+05	2.30E−01	3.76E−03	4.25	0.37	16.50
TA0909	1555	7.91E+07	2.70E+05	2.52E−01	3.34E−03	5.05	0.49	32.95
TA0909	1655	1.25E+08	4.40E+05	2.56E−01	3.55E−03	6.93	0.51	22.37
TA0968	1485	1.15E+07	8.70E+05	4.47E−01	4.84E−02	1.06	0.52	33.21
TA0968	1690	3.03E+07	2.19E+05	4.65E−01	6.82E−03	3.13	0.68	44.50
TA0968	1790	4.99E+07	5.26E+05	3.57E−01	8.12E−03	3.72	0.21	34.55
TA0968	1890	7.16E+07	4.54E+05	3.56E−01	5.40E−03	4.05	0.16	34.00
TA0968	1990	1.01E+08	5.47E+05	3.74E−01	5.25E−03	5.94	0.13	35.18
TA0969	1415	1.06E+07	4.76E+05	4.10E−01	3.03E−02	1.13	0.56	19.21
TA0969	1620	2.97E+07	2.71E+05	4.24E−01	7.14E−03	2.86	0.69	41.65
TA0969	1720	5.07E+07	4.85E+05	2.43E−01	1.06E−02	4.16	0.48	11.19
TA0969	1820	7.26E+07	3.13E+05	3.26E−01	4.05E−03	5.31	0.12	25.04
TA0969	1920	1.04E+08	6.23E+05	3.44E−01	5.37E−03	1.81	0.14	25.07
TA0970	1400	1.02E+07	1.74E+06	3.89E−01	1.00E−01	1.24	0.64	2.91
TA0970	1575	2.80E+07	2.52E+05	3.76E−01	7.26E−03	2.63	0.55	40.18
TA0970	1675	4.96E+07	1.82E+05	2.69E−01	3.58E−03	3.47	0.46	41.39
TA0970	1775	7.48E+07	2.62E+05	2.72E−01	3.42E−03	4.17	0.47	39.40
TA0970	1875	1.11E+08	3.66E+05	2.71E−01	3.31E−03	2.52	0.49	43.34
TA0971	1430	1.07E+07	6.07E+05	3.14E−01	3.28E−02	2.99	0.36	38.71
TA0971	1645	3.06E+07	1.45E+05	3.35E−01	4.09E−03	3.13	0.54	47.02
TA0971	1745	4.98E+07	1.31E+05	2.58E−01	2.77E−03	4.53	0.51	45.63
TA0971	1845	7.06E+07	2.21E+05	2.83E−01	3.14E−03	3.98	0.61	30.82
TA0971	1945	1.03E+08	2.55E+05	2.75E−01	2.60E−03	5.28	0.58	44.04
TA0972	1390	1.07E+07	1.05E+05	3.40E−01	7.94E−03	1.80	0.65	44.42
TA0972	1590	2.82E+07	1.25E+05	3.95E−01	4.12E−03	2.67	1.15	81.65
TA0972	1690	4.90E+07	1.30E+05	2.75E−01	2.68E−03	3.34	0.49	30.78
TA0972	1790	7.24E+07	1.66E+05	2.77E−01	2.35E−03	3.61	0.55	61.65
TA0972	1890	1.03E+08	4.16E+05	3.27E−01	3.46E−03	5.12	0.22	65.59
TA0973	1420	1.05E+07	4.17E+04	2.59E−01	3.67E−03	2.82	0.48	7.86
TA0973	1640	3.13E+07	1.75E+05	3.18E−01	4.45E−03	3.23	0.48	37.18
TA0973	1740	5.03E+07	1.28E+05	2.43E−01	2.55E−03	3.73	0.46	38.61
TA0973	1840	7.16E+07	1.89E+05	2.58E−01	2.55E−03	3.65	0.54	37.90
TA0973	1940	1.01E+08	2.75E+05	2.78E−01	2.78E−03	4.88	0.50	71.54
TA0999	1310	1.05E+07	4.00E+04	2.61E−01	3.44E−03	2.69	0.49	30.32
TA0999	1495	2.91E+07	8.84E+04	3.03E−01	2.95E−03	3.22	0.52	63.45
TA0999	1595	5.04E+07	1.17E+05	2.31E−01	2.37E−03	3.90	0.45	32.76
TA0999	1695	7.50E+07	1.63E+05	2.65E−01	2.19E−03	4.10	0.58	51.75
TA0999	1795	1.12E+08	2.73E+05	2.74E−01	2.41E−03	3.02	0.57	65.22
TA1000	1260	1.08E+07	4.66E+04	2.80E−01	3.84E−03	2.37	0.52	40.67
TA1000	1420	2.68E+07	1.05E+05	3.29E−01	3.76E−03	3.06	0.56	54.85
TA1000	1520	4.92E+07	1.14E+05	2.53E−01	2.24E−03	3.39	0.50	58.73
TA1000	1620	7.62E+07	1.75E+05	2.62E−01	2.24E−03	4.37	0.53	59.30
TA1000	1720	1.13E+08	3.40E+05	3.31E−01	2.72E−03	4.85	0.16	80.98
TA1001	1280	1.06E+07	3.07E+04	3.58E−01	2.77E−03	2.73	0.49	34.96
TA1001	1445	2.84E+07	1.03E+05	3.43E−01	3.48E−03	3.16	0.55	63.60
TA1001	1545	5.04E+07	1.22E+05	2.60E−01	2.46E−03	3.64	0.50	66.70
TA1001	1645	7.51E+07	2.07E+05	3.04E−01	2.73E−03	4.55	0.76	52.23
TA1001	1745	1.12E+08	3.64E+05	3.42E−01	3.12E−03	5.19	0.84	46.68
TA1002	1480	1.00E+07	8.86E+04	2.95E−01	7.31E−03	3.01	0.65	18.87
TA1002	1720	3.19E+07	1.61E+05	3.57E−01	3.80E−03	3.25	0.22	67.23
TA1002	1820	5.01E+07	1.10E+05	2.61E−01	2.25E−03	6.93	0.56	67.87
TA1002	1920	6.84E+07	1.59E+05	2.76E−01	2.31E−03	3.59	0.56	69.49
TA1002	2020	9.61E+07	2.51E+05	2.97E−01	2.61E−03	3.65	0.54	82.87

Figure 5.4: Charge response measurement all data vol.4

Modelturm	HV	Gain	Error	ChargeRes	Error	PVratio	qtau/q0	pe/q0
TA1105	1300	1.05E+07	7.36E+04	2.69E-01	5.74E-03	2.41	0.57	16.24
TA1105	1480	2.85E+07	1.32E+05	3.42E-01	3.59E-03	3.30	0.19	56.26
TA1105	1580	5.03E+07	1.04E+05	2.30E-01	2.10E-03	4.04	0.50	63.78
TA1105	1680	7.74E+07	1.66E+05	2.49E-01	2.09E-03	4.71	0.55	56.47
TA1105	1780	1.17E+08	2.36E+05	2.51E-01	2.06E-03	6.66	0.54	66.42
TA1106	1390	1.07E+07	4.08E+04	2.63E-01	3.48E-03	2.22	0.47	36.67
TA1106	1600	3.07E+07	9.87E+04	3.04E-01	2.88E-03	2.73	0.50	68.11
TA1106	1700	4.97E+07	1.11E+05	2.44E-01	2.20E-03	3.40	0.48	61.14
TA1106	1800	7.28E+07	1.59E+05	2.45E-01	2.15E-03	3.97	0.50	65.47
TA1106	1900	1.02E+08	3.74E+05	2.94E-01	3.11E-03	4.96	0.23	71.36
TA1107	1390	1.05E+07	2.15E+05	4.87E-01	1.98E-02	2.00	0.80	35.15
TA1107	1610	3.42E+07	2.09E+05	4.76E-01	5.55E-03	2.73	0.61	98.00
TA1107	1710	5.40E+07	2.49E+05	4.07E-01	5.09E-03	3.35	0.65	74.98
TA1107	1810	7.92E+07	3.48E+05	4.04E-01	5.13E-03	3.74	0.71	72.05
TA1107	1910	1.04E+08	6.75E+05	4.86E-01	1.98E-02	4.27	0.57	94.24
TA1108	1375	1.08E+07	7.15E+04	3.28E-01	5.70E-03	2.40	0.53	49.04
TA1108	1570	2.85E+07	1.45E+05	4.25E-01	4.11E-03	3.13	0.14	72.51
TA1108	1670	4.99E+07	1.52E+05	2.94E-01	3.05E-03	3.29	0.48	67.99
TA1108	1770	7.18E+07	2.51E+05	3.30E-01	3.14E-03	3.88	0.19	67.17
TA1108	1870	1.03E+08	3.35E+05	3.59E-01	2.94E-03	5.28	0.14	75.11
TA1109	1300	1.04E+07	4.85E+04	2.84E-01	4.13E-03	2.56	0.50	40.12
TA1109	1500	3.13E+07	1.25E+05	3.28E-01	3.36E-03	2.87	0.50	59.28
TA1109	1600	4.94E+07	1.70E+05	3.83E-01	3.19E-03	3.29	0.38	0.14
TA1109	1700	8.22E+07	2.11E+05	2.66E-01	2.51E-03	4.64	0.51	53.08
TA1109	1800	1.26E+08	3.28E+05	2.75E-01	2.67E-03	5.18	0.54	54.41
TA1110	1290	1.04E+07	9.04E+04	2.56E-01	7.22E-03	3.09	0.56	12.48
TA1110	1475	2.82E+07	1.18E+05	3.21E-01	3.98E-03	3.52	0.58	43.80
TA1110	1575	5.11E+07	1.04E+05	2.26E-01	2.10E-03	4.22	0.51	0.13
TA1110	1675	7.83E+07	1.69E+05	2.42E-01	2.15E-03	4.84	0.56	49.52
TA1110	1775	1.18E+08	2.41E+05	2.50E-01	2.08E-03	5.95	0.61	58.03
TA1135	1370	1.04E+07	7.34E+04	3.04E-01	6.20E-03	2.90	0.63	21.93
TA1135	1565	2.96E+07	1.26E+05	3.43E-01	3.89E-03	3.47	0.63	52.68
TA1135	1665	4.96E+07	1.15E+05	2.60E-01	2.42E-03	4.38	0.52	62.77
TA1135	1765	7.30E+07	1.63E+05	2.61E-01	2.25E-03	4.26	0.58	54.52
TA1135	1865	1.04E+08	3.66E+05	3.14E-01	3.26E-03	5.25	0.22	58.43
TA1137	1290	1.07E+07	1.13E+05	4.16E-01	1.01E-02	2.35	1.07	37.34
TA1137	1450	2.73E+07	2.67E+05	4.61E-01	8.89E-03	2.95	0.07	31.46
TA1137	1550	5.06E+07	2.20E+05	3.20E-01	4.34E-03	3.40	0.49	52.22
TA1137	1650	7.66E+07	4.46E+05	3.42E-01	5.28E-03	3.88	0.60	35.76
TA1137	1750	1.18E+08	4.33E+05	3.76E-01	3.12E-03	4.69	0.23	74.08
TA1138	1305	9.46E+06	8.61E+05	3.99E-01	4.79E-02	1.94	0.47	19.12
TA1138	1535	3.03E+07	2.55E+05	5.01E-01	6.86E-03	2.53	0.60	80.80
TA1138	1635	5.08E+07	4.03E+05	4.07E-01	6.48E-03	2.89	0.60	70.00
TA1138	1735	7.97E+07	4.39E+05	3.81E-01	5.31E-03	3.72	0.59	47.35
TA1138	1835	1.16E+08	6.33E+05	4.20E-01	5.52E-03	4.30	0.80	59.31
TA1140	1385	1.05E+07	4.48E+04	3.58E-01	3.99E-03	2.66	0.36	0.68
TA1140	1570	2.94E+07	1.09E+05	3.37E-01	3.52E-03	2.98	0.51	63.76
TA1140	1670	4.91E+07	1.23E+05	2.56E-01	2.58E-03	3.49	0.50	53.60
TA1140	1770	6.70E+07	1.44E+05	3.54E-01	2.97E-03	4.49	0.26	68.38
TA1140	1870	1.04E+08	3.70E+05	3.19E-01	3.17E-03	4.84	0.20	66.85

Figure 5.5: Charge response measurement all data vol.5

PMT_Name	HV	Waveform		Noise Rate [Hz]							
		Sigma[ns]	Error[ns]	100ns	500ns	800ns	1us	3us	5us	8us	10us
TA0348	1955	1.96	0.15	1447	1077	1066	1057	1062	880	767	708
TA0349	1775	2.26	0.16	1224	1107	1027	1040	856	742	618	620
TA0350	1745	2.04	0.16	1272	1093	983	993	801	746	635	594
TA0352	1620	2.22	0.16	947	910	859	776	696	671	594	564
TA0356	1860	1.95	0.14	883	733	707	669	688	575	550	514
TA0357	2090	1.95	0.14	1343	1081	1058	982	814	757	626	603
TA0523	1690	2.08	0.16	914	870	862	754	693	616	556	508
TA0526	1881	2.09	0.17	968	879	848	789	722	694	654	618
TA0528	1970	1.97	0.18	887	841	812	733	702	654	564	552
TA0529	1760	2.08	0.18	977	870	806	793	695	668	619	579
TA0530	2135	1.97	0.27	1311	1047	998	939	781	765	652	584
TA0538	1650	2.08	0.16	723	718	602	610	553	500	461	452
TA0433	1800	2.21	0.18	1779	1675	1488	1333	1110	1075	1032	988
TA0435	1805	2.33	0.18	956	884	841	834	755	656	613	586
TA0438	1640	2.26	0.17	1508	1460	1391	1323	1217	1115	1029	970
TA0451	1860	2.17	0.15	909	846	778	831	757	746	699	620
TA0452	2115	2.14	0.13	1146	982	945	980	823	737	664	622
TA0464	1860	2.19	0.17	1101	997	919	913	809	747	666	626
TA0593	1915	2.25	0.19	1563	1387	1366	1400	972	953	893	740
TA0594	1895	2.17	0.16	1981	1910	1917	1891	1610	1453	1303	1328
TA0595	1860	2.20	0.17	1085	981	938	914	805	755	659	626
TA0596	1700	2.22	0.16	1019	912	858	832	730	660	617	583
TA0597	1710	2.23	0.18	708	635	593	571	520	506	484	475
TA0598	1680	2.18	0.16	1076	1047	987	969	883	799	768	713
TA0664	1635	2.23	0.22	741	709	694	685	671	633	629	613
TA0665	1780	1.85	0.13	853	807	737	724	640	601	556	521
TA0666	1835	1.88	0.15	943	907	784	739	703	649	577	536
TA0772	1550	2.15	0.16	1042	976	904	882	776	727	617	599
TA0773	1605	2.10	0.16	1085	980	800	791	727	693	625	620
TA0774	1790	2.06	0.16	1129	933	865	829	744	671	623	595
TA0781	1660	2.08	0.14	1362	1227	1143	1086	982	842	727	681
TA0898	1890	2.04	0.15	1159	1081	978	947	840	826	710	662
TA0901	1640	2.05	0.15	804	794	693	684	643	637	585	571
TA0902	1615	2.04	0.14	1095	963	870	820	816	744	664	635
TA0907	1580	2.13	0.15	988	876	866	861	764	727	661	648
TA0908	1670	2.11	0.17	990	887	867	816	755	651	606	591
TA0909	1455	2.13	0.16	1143	970	880	835	822	713	623	593
TA0968	1790	2.03	0.15	1295	1239	1126	1093	853	751	677	644
TA0969	1720	2.08	0.14	1119	1070	998	976	842	813	736	680
TA0970	1675	2.12	0.16	1181	1067	970	937	798	750	672	604
TA0971	1745	2.14	0.16	894	830	770	765	681	652	591	542
TA0972	1790	2.05	0.14	1115	1056	1045	1029	822	775	717	670
TA0973	1740	2.10	0.15	1000	879	824	786	654	611	540	514
TA0999	1595	2.18	0.16	944	891	780	773	724	649	617	557
TA1000	1520	2.11	0.15	923	898	871	829	726	684	624	556
TA1001	1545	2.16	0.18	1122	981	971	966	764	737	702	652
TA1002	1820	2.09	0.15	1119	999	915	863	847	764	681	670
TA1105	1580	2.20	0.17	1316	1232	1121	1096	990	882	822	736
TA1106	1700	2.11	0.15	1379	1164	1135	1018	923	767	664	626
TA1107	1710	2.17	0.18	1195	1093	1119	1029	923	870	796	744
TA1108	1670	2.14	0.16	1285	1016	1006	917	821	798	696	669
TA1109	1600	2.13	0.15	1071	976	925	925	830	766	652	627
TA1110	1575	2.10	0.14	1217	1111	1100	1029	935	891	820	750
TA1135	1665	2.10	0.14	1131	912	889	901	727	684	604	595
TA1137	1550	2.16	0.15	962	905	819	799	759	668	631	594
TA1138	1635	2.06	0.15	967	944	904	919	792	735	681	651
TA1140	1670	2.18	0.17	1100	985	936	901	802	686	642	606

Figure 5.6: This table is all data of measured waveform data and noise rate. Cell painted out that pink is more than 1000 [Hz] of noise rate, yellow's cell is 750 ~ 1000 [Hz], green's is 500 ~ 750 [Hz] and blue's is less than 500 [Hz]

44